Iterative Adaptive Approaches to MIMO Radar Imaging

William Roberts, *Student Member, IEEE*, Petre Stoica, *Fellow, IEEE*, Jian Li*, *Fellow, IEEE*, Tarik Yardibi, *Student Member, IEEE*, and Firooz A. Sadjadi

***Abstract*—Multiple-input multiple-output (MIMO) radar can achieve superior performance through waveform diversity over conventional phased-array radar systems. When a MIMO radar transmits orthogonal waveforms, the reflected signals from scatterers are linearly independent of each other. Therefore, adaptive receive filters, such as Capon and amplitude and phase estimation (APES) filters, can be directly employed in MIMO radar applications. High levels of noise and strong clutter, however, significantly worsen detection performance of the data-dependent beamformers due to a shortage of snapshots. The iterative adaptive approach (IAA), a non-parametric and user parameter-free weighted least-squares algorithm, was recently shown to offer improved resolution and interference rejection performance in several passive and active sensing applications. In this paper, we show how IAA can be extended to MIMO radar imaging, in both the negligible and non-negligible intra-pulse Doppler cases, and we also establish some theoretical convergence properties of IAA. In addition, we propose a regularized IAA algorithm, referred to as IAA-R, which can perform better than IAA by accounting for unrepresented additive noise terms in the signal model. Numerical examples are presented to demonstrate the superior performance of MIMO radar over single-input multiple-output (SIMO) radar, and further highlight the improved performance achieved with the proposed IAA-R method for target imaging.**

***Index Terms*—MIMO radar, phased-array radar, iterative adaptive approach (IAA), regularized IAA, radar imaging, intra-pulse Doppler.**

I. Introduction

A multiple-input multiple-output (MIMO) antenna array system can be used in radar applications to provide higher resolution and better sensitivity (for detecting slowly-moving targets) than a phased-array radar system (see, e.g., [1]-[12] and the references therein). The waveform diversity afforded by the MIMO radar can serve to increase the flexibility at the transmitter [6]-[12]. For example, probing signals can be designed to approximate a desired transmit beampattern and to minimize undesirable cross-correlation terms (see, e.g., [13]-[17] and the references therein). When orthogonal waveforms are transmitted, the parameter identifiability of the radar, meaning the maximum number of targets that can be uniquely identified, is vastly improved. With careful construction of the radar's antenna structure, in fact, the parameter identifiability can be increased by a factor of M, where M is the number of transmitting antennas, over the corresponding phased-array system [18]. Furthermore, when the radar transmits M orthogonal waveforms, the virtual array of the radar system is a filled array with an aperture length up to M times that of the receive array [10], [11]. This advantage of MIMO radar can be exploited to achieve an M-fold improvement in the spatial imaging resolution over the conventional phased-array radar [10], [11].

In this paper, we consider MIMO radar imaging. The goal of radar imaging is to provide an estimate of the radar cross sections (RCS) of targets at precise angular locations and distances relative to the radar. When motion (either of the radar or of targets within a scene of interest) is present, the relative speeds of objects can also be estimated through Doppler considerations.

Irrespective of the array system, data-independent approaches, such as delay-and-sum (DAS) (or matched filtering), can be used for radar imaging. However, DAS suffers from low resolution and high sidelobe level problems. With a narrowband MIMO radar, orthogonal waveforms from the transmit antennas hit targets in the scene of interest at different time instants, thus undergoing different phase shifts. Therefore, the reflected signals at the receiver are linearly independent of each other when the number of targets per range and Doppler bin is less than or equal to the number of orthogonal probing waveforms. Due to this independence, adaptive beamforming techniques, which fail to work with coherent or highly correlated signals, can be effectively employed to estimate target parameters with MIMO radar systems [19]. The existing adaptive approaches, such as Capon [20] and amplitude and phase estimation (APES) [21], can be used to mitigate clutter effects and improve resolution over conventional DAS. When noise (and clutter) levels in the received signal are high, however, the performance of data-dependent approaches might degrade significantly unless the number of snapshots is rather

This material is based upon work supported in part by the SMART fellowship program, the Army Research Office under Grant No. W911NF-07-1-0450, the National Science Foundation under Grant No. CCF-0634786, the National Aeronautics and Space Administration (NASA) under Grant No. NNX07AO15A, the Swedish Research Council (VR), and the European Research Council (ERC). Opinions, interpretations, conclusions, and recommendations are those of the authors and are not necessarily endorsed by the United States Government.

William Roberts and Tarik Yardibi are with the Department of Electrical and Computer Engineering, University of Florida, Gainesville, FL 32611-6130, USA. Email: wroberts83@hotmail.com and ytarik@dsp.ufl.edu.

*Jian Li is with the Department of Electrical and Computer Engineering, University of Florida, Gainesville, FL 32611-6130, USA. Phone: (352) 392-2642; Fax: (352) 392-0044; Email: li@dsp.ufl.edu. Please address all correspondence to Jian Li.

Petre Stoica is with the Department of Information Technology, Uppsala University, Uppsala, Sweden. Phone: 46-18-471-7619; Fax: 46-18-511925; Email: ps@it.uu.se.

Firooz A. Sadjadi is with Lockheed Martin Corp, 3333 Pilot Knob Road, Eagan, MN 55121, USA. Email: firooz.a.sadjadi@lmco.com.

large.

Recently, a non-parametric and user parameter-free algorithm, referred to as the iterative adaptive approach (IAA),[1] was presented for applications including passive array processing, multiple-input single-output (MISO) communication channel estimation and single antenna radar systems [22] . IAA was shown to perform well for cases of few or even a single snapshot and closely-spaced sources, and it was shown to outperform existing sparse signal reconstruction algorithms. In [25], IAA was extended to the case of spectral analysis for non-uniformly sampled real-valued data, and was shown to attain significantly better performance than the traditional periodogram approach to spectral estimation. IAA was further adapted to single antenna range-Doppler imaging in [26], specifically for the case when the transmitted signal is a train of probing pulses. Improved resolution was achieved using IAA compared to that obtained using a data-independent instrumental variables (IV) filter.

Previous descriptions of IAA for radar imaging have been restricted to the single antenna case. In this paper, we broaden the application of IAA to include MIMO antenna arrays and demonstrate the superior imaging performance of MIMO radar over its phased-array counterpart. In Section II, we extend IAA for MIMO radar applications in the negligible intra-pulse Doppler case, and in Section III, we incorporate intra-pulse Doppler effects into the algorithm. In Section IV, we propose the regularized IAA algorithm, namely IAA-R, which improves the robustness of IAA by explicitly accounting for the additive noise terms. By assuming a statistical model of the received signal, we derive the maximum likelihood based version of IAA-R (IAA-R-ML) in Section V. We show that IAA-R can be viewed as an approximation to IAA-R-ML, which is guaranteed to be locally convergent. We also provide a theoretical local convergence analysis of IAA (in the appendix). Numerical simulations, which we present in Section VI, demonstrate the superior performance of a MIMO system over that of a single-input multiple-output (SIMO) antenna array system, as well as the superior performance of IAA-R over DAS and several data-adaptive beamforming techniques. Also, the advantages of IAA-R over IAA, for MIMO radar applications, are highlighted. Conclusions are provided in Section VII.

$Notation$: We denote vectors and matrices by boldface lowercase and uppercase letters, respectively. $\|\cdot\|_2$ denotes the Euclidean norm, $\|\cdot\|_{\mathrm{F}}^2$ denotes the matrix Frobenius norm, $(\cdot)^T$ denotes the transpose operation, $(\cdot)^*$ denotes the conjugate transpose operation, vec$(\cdot)$ refers to the vectorization operation (i.e, stacking the columns of a matrix on top of each other), tr$(\cdot)$ denotes the trace operation, $\odot$ denotes the Hadamard (elementwise) matrix product, $|\cdot|$ refers to the determinant operation, and $\mathbf{I}_N$ represents the $N \times N$ identity matrix. $\mathbf{R} \in \mathbb{R}^{L\times M}$ and $\mathbf{R} \in \mathbb{C}^{L\times M}$ denote a real and complex-valued $L \times M$ matrix $\mathbf{R}$, respectively. $\hat{\alpha}$ denotes the estimate of the parameter α.

[1]Note that the algorithm was named as IAA-APES in [22]. Herein, we refer to the algorithm as IAA for conciseness.

II. Negligible Doppler Case

This section formulates the MIMO spotlight synthetic aperture radar (SAR) [27] imaging problem and describes how IAA can be extended to estimate the target parameters, specifically the amplitude, range, and angle of each target present. The targets are assumed to be stationary and therefore the intra-pulse Doppler effects are neglected. The non-negligible Doppler case will be analyzed in the next section.

A. Problem Formulation

Consider a MIMO radar system with M transmit antennas and N receive antennas. Let

$$\mathbf{x}_m = \begin{bmatrix} x_m(1) & \dots & x_m(L) \end{bmatrix}^T, \quad m = 1, \dots, M, \quad (1)$$

represent the length L transmitted signal from the mth transmit antenna. Let

$$\mathbf{X} = \begin{bmatrix} \mathbf{x}_1 & \mathbf{x}_2 & \dots & \mathbf{x}_M \end{bmatrix} \quad (2)$$

consist of the transmitted signals from all the transmit antennas ($\mathbf{X} \in \mathbb{C}^{L\times M}$). Further, let

$$\tilde{\mathbf{X}} = \begin{bmatrix} \mathbf{X} \\ \mathbf{0}_{(P-1)\times M} \end{bmatrix}, \quad (3)$$

where $\tilde{\mathbf{X}} \in \mathbb{C}^{(L+P-1)\times M}$ denotes the zero-appended transmitted waveform matrix, $\mathbf{0}_{(P-1)\times M}$ is a $(P-1)\times M$ matrix of zeros, and $P-1$ refers to the maximum delay (in sampling intervals) between the reflected signals from various range bins and the first received signal (from the closest range bin to the radar). For a radar collecting data from $\tilde{N}$ positions, the received signal from collection position n, that is synchronized with the arrival of the first reflected signal, can be expressed as:

$$\mathbf{D}^*(n) = \sum_{p=1}^{P}\sum_{k=1}^{K} \alpha_{p,k}\mathbf{a}_k(n)\mathbf{b}_k^T(n)\tilde{\mathbf{X}}^*\mathbf{J}_p + \mathbf{E}^*(n), \quad n = 1, \dots, \tilde{N}, \quad (4)$$

where the complex scattering coefficients of the targets, which are directly proportional to their corresponding radar cross section (RCS), are represented by $\{\alpha_{p,k}\}$, p denotes the range index, k denotes the angle index, K is the number of potential scatterers in each range bin and $\{\mathbf{E}(n)\}$ represents the additive noise. The terms $\{\mathbf{a}_k(n)\}$ and $\{\mathbf{b}_k(n)\}$ refer to the receive and transmit steering vectors, respectively. For uniform linear arrays, they can be described by:

$$\mathbf{a}_k(n) = \begin{bmatrix} e^{-\frac{j2\pi((n-1)d_n)\sin(\theta_k)}{\lambda_0}} & e^{-\frac{j2\pi((n-1)d_n+d_r)\sin(\theta_k)}{\lambda_0}} & \dots & e^{-\frac{j2\pi((n-1)d_n+(N-1)d_r)\sin(\theta_k)}{\lambda_0}} \end{bmatrix}^T, \quad (5)$$

and

$$\mathbf{b}_k(n) = \begin{bmatrix} e^{-\frac{j2\pi((n-1)d_n)\sin(\theta_k)}{\lambda_0}} & e^{-\frac{j2\pi((n-1)d_n+d_t)\sin(\theta_k)}{\lambda_0}} & \dots & e^{-\frac{j2\pi((n-1)d_n+(M-1)d_t)\sin(\theta_k)}{\lambda_0}} \end{bmatrix}^T, \quad (6)$$

where d_t and d_r refer to the distances between adjacent transmitting and receiving antennas, respectively, λ_0 represents the carrier wavelength of the radar system, d_n refers to the separation between collection positions, and θ_k denotes the impinging angle (relative to the array normal) of targets in the kth angle bin. Finally, $\mathbf{J}_p \in \mathbb{R}^{(L+P-1)\times(L+P-1)}$ is a shift matrix used to describe the received signals from different range bins, and it can be written as:

$$\mathbf{J}_p = \begin{bmatrix} \overbrace{\begin{matrix} & & 1 \\ & \iddots & \\ 1 & & \end{matrix}}^{p} & \mathbf{0} \\ \mathbf{0} & \begin{matrix} & & \\ & \ddots & \\ & & 1 \end{matrix} \end{bmatrix}. \tag{7}$$

Note that

$$\tilde{\mathbf{X}}^*\mathbf{J}_p = \begin{bmatrix} \overbrace{0 \;\cdots\; 0 \; x_1^*(1)}^{p} & \cdots & x_1^*(L) & 0 & \cdots & 0 \\ \vdots & & \vdots & & & \vdots \\ 0 \;\cdots\; 0 \; x_M^*(1) & \cdots & x_M^*(L) & 0 & \cdots & 0 \end{bmatrix}, \quad p = 1, \ldots, P. \tag{8}$$

To further simplify notation, we accumulate the received signals from each of the look positions as:

$$\mathbf{d} = \begin{bmatrix} \mathrm{vec}(\mathbf{D}^*(1)) \\ \vdots \\ \mathrm{vec}(\mathbf{D}^*(\tilde{N})) \end{bmatrix}. \tag{9}$$

In a similar way, we can define a matrix $\mathbf{Y}$ that contains the known quantities (the steering vectors, the transmit waveforms and the shift matrix) in the received signal as follows:

$$\mathbf{Y} = \begin{bmatrix} \mathbf{y}_{1,1} & \ldots & \mathbf{y}_{1,K} & \mathbf{y}_{2,1} & \ldots & \mathbf{y}_{P,K} \end{bmatrix}, \tag{10}$$

where

$$\mathbf{y}_{p,k} = \begin{bmatrix} \tilde{\mathbf{y}}_{p,k}(1) \\ \vdots \\ \tilde{\mathbf{y}}_{p,k}(\tilde{N}) \end{bmatrix}, \quad p = 1, \ldots, P, \quad k = 1, \ldots, K, \tag{11}$$

and

$$\tilde{\mathbf{y}}_{p,k}(n) = \mathrm{vec}\left[\mathbf{a}_k(n)\mathbf{b}_k^T(n)\tilde{\mathbf{X}}^*\mathbf{J}_p\right], \quad p = 1, \ldots, P, \quad k = 1, \ldots, K, \quad n = 1, \ldots, \tilde{N}. \tag{12}$$

Consequently, by using (10)-(11), (9) can be expressed as:

$$\mathbf{d} = \mathbf{Y}\boldsymbol{\alpha} + \mathbf{e}, \tag{13}$$

where

$$\boldsymbol{\alpha} = \begin{bmatrix} \alpha_{1,1} & \ldots & \alpha_{1,K} & \alpha_{2,1} & \ldots & \alpha_{P,K} \end{bmatrix}^T, \tag{14}$$

and

$$\mathbf{e} = \begin{bmatrix} \mathrm{vec}(\mathbf{E}^*(1)) \\ \vdots \\ \mathrm{vec}(\mathbf{E}^*(\tilde{N})) \end{bmatrix}. \tag{15}$$

The problem of interest, then, is to accurately estimate the target reflection coefficients $\boldsymbol{\alpha}$ from the measurement vector $\mathbf{d}$ and known matrix $\mathbf{Y}$.

The DAS estimates of the target parameters are given by:

$$\hat{\alpha}_{p,k} = \frac{\mathbf{y}_{p,k}^*\mathbf{d}}{\mathbf{y}_{p,k}^*\mathbf{y}_{p,k}}, \quad p = 1, \ldots, P, \quad k = 1, \ldots, K. \tag{16}$$

The basic assumption behind DAS is that $\mathbf{y}_{p,k}^*\mathbf{y}_{p,k}$ is relatively large compared to $\mathbf{y}_{p,k}^*\mathbf{y}_{p',k'}$, where $(p',k') \neq (p,k)$, $p' = 1, \ldots, P$ and $k' = 1, \ldots, K$, so that the signal-of-interest is passed undistorted while the contribution from the interfering signals is reduced. In other words, in order for DAS to work properly, the columns of $\mathbf{Y}$ should be close to being orthogonal. However, this condition is rarely satisfied in practice and hence DAS usually suffers from high sidelobe level and low resolution problems.

B. IAA

IAA iteratively refines the DAS target estimates to achieve higher resolution and better interference suppression. Here, we show how IAA can be extended to estimate the target parameters in the MIMO radar problem defined in (13) (we still refer to the extended algorithm as IAA for simplicity).

Let the target parameter of interest be $\alpha_{p,k}$. Treating the possible targets corresponding to $\{\alpha_{p',k'}\}$, where $(p',k') \neq (p,k)$, $p' = 1, \ldots, P$ and $k' = 1, \ldots, K$, as interferences, we define the interference covariance matrix as:

$$\mathbf{Q}_{p,k} = \sum_{\substack{p'=1 \\ (p',k')\neq(p,k)}}^{P} \sum_{k'=1}^{K} |\alpha_{p',k'}|^2 \mathbf{y}_{p',k'}\mathbf{y}_{p',k'}^*, \quad p = 1, \ldots, P, \;\; k = 1, \ldots, K. \tag{17}$$

The data covariance matrix is defined as:

$$\mathbf{R} = \sum_{p=1}^{P}\sum_{k=1}^{K} |\alpha_{p,k}|^2 \mathbf{y}_{p,k}\mathbf{y}_{p,k}^*, \tag{18}$$

where $\mathbf{R} \in \mathbb{C}^{(N\tilde{N}(L+P-1))\times(N\tilde{N}(L+P-1))}$.

IAA minimizes the following weighted least-squares cost function (see, e.g., [28], [29]) with respect to the reflection coefficient, $\alpha_{p,k}$, of the target of interest:

$$(\mathbf{d} - \alpha_{p,k}\mathbf{y}_{p,k})^*\mathbf{Q}_{p,k}^{-1}(\mathbf{d} - \alpha_{p,k}\mathbf{y}_{p,k}). \tag{19}$$

The minimization of (19) yields the following estimate for the target parameters:

$$\hat{\alpha}_{p,k} = \frac{\mathbf{y}_{p,k}^*\mathbf{Q}_{p,k}^{-1}\mathbf{d}}{\mathbf{y}_{p,k}^*\mathbf{Q}_{p,k}^{-1}\mathbf{y}_{p,k}}, \quad p = 1, \ldots, P, \;\; k = 1, \ldots, K. \tag{20}$$

Noting that

$$\mathbf{Q}_{p,k} = \mathbf{R} - |\alpha_{p,k}|^2 \mathbf{y}_{p,k}\mathbf{y}_{p,k}^*, \tag{21}$$

and applying the matrix inversion lemma to (21) (see, e.g., [29]) yield,

$$\mathbf{y}_{p,k}^*\mathbf{Q}_{p,k}^{-1} = \frac{\mathbf{y}_{p,k}^*\mathbf{R}^{-1}}{1 - |\alpha_{p,k}|^2\mathbf{y}_{p,k}^*\mathbf{R}^{-1}\mathbf{y}_{p,k}}. \tag{22}$$

TABLE I
IAA FOR MIMO SAR IMAGING.

initialize

$$\hat{\alpha}_{p,k} = \frac{\mathbf{y}_{p,k}^* \mathbf{d}}{\mathbf{y}_{p,k}^* \mathbf{y}_{p,k}}, \quad p = 1, \ldots, P, \quad k = 1, \ldots, K$$

repeat

$$\mathbf{R} = \sum_{p=1}^{P} \sum_{k=1}^{K} |\hat{\alpha}_{p,k}|^2 \mathbf{y}_{p,k} \mathbf{y}_{p,k}^*$$

$$\hat{\alpha}_{p,k} = \frac{\mathbf{y}_{p,k}^* \mathbf{R}^{-1} \mathbf{d}}{\mathbf{y}_{p,k}^* \mathbf{R}^{-1} \mathbf{y}_{p,k}}, \quad p = 1, \ldots, P, \quad k = 1, \ldots, K$$

until (a certain number of iterations is reached)

Consequently, $\mathbf{Q}_{p,k}^{-1}$ in (20) can be replaced with $\mathbf{R}^{-1}$, which needs to be computed only once. The IAA estimate of $\alpha_{p,k}$ then becomes:

$$\hat{\alpha}_{p,k} = \frac{\mathbf{y}_{p,k}^* \mathbf{R}^{-1} \mathbf{d}}{\mathbf{y}_{p,k}^* \mathbf{R}^{-1} \mathbf{y}_{p,k}}, \quad p = 1, \ldots, P, \ \ k = 1, \ldots, K. \quad (23)$$

Since $\mathbf{R}$ depends on $\{\alpha_{p,k}\}$, which are unknown, IAA is implemented as an iterative algorithm and the DAS estimates are used for initializing IAA. For most practical applications, convergence occurs after typically no more than 10 iterations [22]. The algorithm is summarized in Table 1. A local convergence analysis of IAA is provided in the appendix. Note that $\mathbf{R}$ in IAA (see (18)) is computed using the previous estimates of the target parameters $\{\alpha_{p,k}\}$ and *not* from the measurements $\mathbf{d}$ as done in adaptive array processing algorithms. Note also that setting $\mathbf{R} = \mathbf{I}_{N\tilde{N}(L+P-1)}$ in (23) results in the DAS estimate.

C. Incorporating BIC

To produce sparsity in the IAA result, the Bayesian information criterion (BIC), a model order selection tool [30], can be used. Given the IAA estimate for a scene, the BIC approach selects a target with range-angle indices $(\tilde{p}, \tilde{k})$, which minimizes the following criterion:

$$\begin{aligned} \mathrm{BIC}_{(\tilde{p},\tilde{k})}(\eta) = {} & 2N\tilde{N}(L+P-1) \\ & \times \ln \left[\left\| \mathbf{d} - \sum_{(p,k) \in \{\mathcal{J}(\eta) \bigcup (\tilde{p},\tilde{k})\}} \mathbf{y}_{p,k} \hat{\alpha}_{p,k} \right\|_2^2 \right] \\ & + 4\eta \ln(2N\tilde{N}(L+P-1)) \,, \quad (24) \end{aligned}$$

where η denotes the number of targets currently selected ($\eta = 1$ for the first iteration). The value of 4 in the penalty term of (24) is chosen to reflect the number of unknowns for each target: amplitude (complex valued), range, and angle. Also, $\mathcal{J}(\eta)$ refers to the set of target indices already selected at the current iteration ($\mathcal{J}(1) = \{\emptyset\}$, where $\{\emptyset\}$ denotes the empty set), and $(\tilde{p}, \tilde{k})$ represents a remaining target point in the scene (i.e., $(\tilde{p}, \tilde{k}) \notin \mathcal{J}(\eta)$). At each iteration of the algorithm, a new target point $(\tilde{p}, \tilde{k})$ is selected such that, along with the set of indices $\mathcal{J}(\eta)$ currently selected, $\mathrm{BIC}_{(\tilde{p},\tilde{k})}(\eta)$ is minimized. This procedure is repeated until the function in (24) does not decrease anymore. Reflection coefficients not present in $\mathcal{J}(\eta)$ at the end of this procedure are set to zero and are assumed not to represent true targets in the scene. Note that the second term on the right side of (24) does not matter to peak selection; it matters only when (24) is used to select the number of peaks to retain.

III. NON-NEGLIGIBLE DOPPLER CASE

This section considers the case of a stationary vertical MIMO array and mobile targets, and further extends IAA to deal with Doppler considerations in a multiple antenna system. In this case, the signal model incorporates Doppler shifts on the received signals and the target parameters of interest are now amplitude, range, angle and Doppler.

A. Problem Formulation

In order to describe IAA for the Doppler-present case, the received signal model has to be reformulated. Denote the received data as $\mathbf{Z}^* \in \mathbb{C}^{N \times (L+P-1)}$, which is synchronized with the arrival of the first reflected signal. $\mathbf{Z}$ can be expressed as:

$$\mathbf{Z}^* = \sum_{p=1}^{P} \sum_{k=1}^{K} \sum_{h=1}^{H} \alpha_{p,k,h} \mathbf{a}_k \mathbf{b}_k^T \tilde{\mathbf{X}}_{\mathrm{D}}^*(\omega_h) \mathbf{J}_p + \mathbf{E}_{\mathrm{D}}^* \,, \quad (25)$$

where "D" is used to denote Doppler, p is the range index, k is the angle index, h is the Doppler index, H denotes the number of bins in the Doppler interval of interest and ω_h denotes the angular Doppler frequency corresponding to the hth Doppler bin, $h = 1, \ldots, H$. The steering vectors, $\{\mathbf{a}_k\}$ and $\{\mathbf{b}_k\}$, and the noise term, $\mathbf{E}_{\mathrm{D}}^*$, are defined similarly to their corresponding terms in (4), except that the dependency on n is removed since the radar is assumed to be stationary (let $n = 1$ in (5) and (6)). The complex scattering coefficients of the targets, $\{\alpha_{p,k,h}\}$, now include a third dimension (indexed by h) to model the targets' speeds. We let

$$\tilde{\mathbf{x}}_m(\omega_h) = \mathbf{x}_m \odot \mathbf{d}(\omega_h) \,, \quad m = 1, \ldots, M, \ \ h = 1, \ldots, H, \quad (26)$$

with $\mathbf{x}_m$ defined in (1), and

$$\mathbf{d}(\omega_h) = \begin{bmatrix} 1 & \mathrm{e}^{j\omega_h} & \ldots & \mathrm{e}^{j\omega_h(L-1)} \end{bmatrix}^T \,, \quad h = 1, \ldots, H. \quad (27)$$

We then define $\tilde{\mathbf{X}}_{\mathrm{D}}(\omega_h)$ similarly to (3) by letting

$$\tilde{\mathbf{X}}_{\mathrm{D}}(\omega_h) = \begin{bmatrix} \mathbf{X}_{\mathrm{D}}(\omega_h) \\ \mathbf{0}_{(P-1)\times M} \end{bmatrix} \,, \quad (28)$$

where $\mathbf{X}$ is replaced by the Doppler shifted signal $\mathbf{X}_{\mathrm{D}}(\omega_h) \in \mathbb{C}^{L \times M}$:

$$\mathbf{X}_{\mathrm{D}}(\omega_h) = \begin{bmatrix} \tilde{\mathbf{x}}_1(\omega_h) & \tilde{\mathbf{x}}_2(\omega_h) & \ldots & \tilde{\mathbf{x}}_M(\omega_h) \end{bmatrix} . \quad (29)$$

To write the signal model given in (25) more compactly, let $\mathbf{z} = \mathrm{vec}(\mathbf{Z}^*)$. $\mathbf{z}$ can then be represented in the following form:

$$\mathbf{z} = \mathbf{Y}_{\mathrm{D}} \boldsymbol{\alpha}_{\mathrm{D}} + \mathbf{e}_{\mathrm{D}} \,, \quad (30)$$

where

$$\mathbf{Y}_{\mathrm{D}} = \begin{bmatrix} \mathbf{y}_{1,1,1} & \mathbf{y}_{1,1,2} & \ldots & \mathbf{y}_{P,K,H} \end{bmatrix} , \quad (31)$$

$$\boldsymbol{\alpha}_{\mathrm{D}} = \begin{bmatrix} \alpha_{1,1,1} & \alpha_{1,1,2} & \ldots & \alpha_{P,K,H} \end{bmatrix}^T , \quad (32)$$

with

$$\mathbf{y}_{p,k,h} = \text{vec}\left[\mathbf{a}_k \mathbf{b}_k^T \tilde{\mathbf{X}}_{\text{D}}^*(\omega_h)\mathbf{J}_p\right] \ , \quad p = 1, \ldots, P, \\ k = 1, \ldots, K, \ \ h = 1, \ldots, H. \quad (33)$$

The complex noise in (30) is simply defined as $\mathbf{e}_{\text{D}} = \text{vec}(\mathbf{E}_{\text{D}}^*)$.

Similarly to (16), the DAS estimate of the target parameters is given by:

$$\hat{\alpha}_{p,k,h} = \frac{\mathbf{y}_{p,k,h}^* \mathbf{z}}{\mathbf{y}_{p,k,h}^* \mathbf{y}_{p,k,h}} \ , \quad p = 1, \ldots, P, \\ k = 1, \ldots, K, \ \ h = 1, \ldots, H. \quad (34)$$

In order for DAS to show good performance, $\mathbf{y}_{p,k,h}^* \mathbf{y}_{p,k,h}$ should be large relative to $\mathbf{y}_{p,k,h}^* \mathbf{y}_{p',k',h'}$, where $(p', k', h') \neq (p, k, h)$, $p' = 1, \ldots, P$, $k' = 1, \ldots, K$, and $h' = 1, \ldots, H$, which is hardly possible in practice.

B. IAA

To describe IAA for a MIMO angle-range-Doppler imaging radar, a similar approach to the one taken in Section II-B will be used. As in (18), we can model the covariance matrix of the received signal by:

$$\mathbf{R}_{\text{D}} = \sum_{p=1}^{P} \sum_{k=1}^{K} \sum_{h=1}^{H} |\alpha_{p,k,h}|^2 \mathbf{y}_{p,k,h} \mathbf{y}_{p,k,h}^* \ , \quad (35)$$

where $\mathbf{R}_{\text{D}} \in \mathbb{C}^{(N(L+P-1))\times(N(L+P-1))}$. We represent the covariance matrix of the interference to the particular target, $\alpha_{p,k,h}$, as:

$$\mathbf{Q}_{p,k,h} = \mathbf{R}_{\text{D}} - |\alpha_{p,k,h}|^2 \mathbf{y}_{p,k,h} \mathbf{y}_{p,k,h}^* \ . \quad (36)$$

We again consider the weighted least-squares cost function:

$$(\mathbf{z} - \alpha_{p,k,h}\mathbf{y}_{p,k,h})^* \mathbf{Q}_{p,k,h}^{-1} (\mathbf{z} - \alpha_{p,k,h}\mathbf{y}_{p,k,h}) \ . \quad (37)$$

Minimization of (37) with respect to the RCS related amplitude of the target of interest $\alpha_{p,k,h}$ yields the update formula:

$$\hat{\alpha}_{p,k,h} = \frac{\mathbf{y}_{p,k,h}^* \mathbf{Q}_{p,k,h}^{-1} \mathbf{z}}{\mathbf{y}_{p,k,h}^* \mathbf{Q}_{p,k,h}^{-1} \mathbf{y}_{p,k,h}} \ , \quad p = 1, \ldots, P, \\ k = 1, \ldots, K, \ \ h = 1, \ldots, H. \quad (38)$$

The matrix inversion lemma can again be used to replace $\mathbf{Q}_{p,k,h}^{-1}$ in (38) with $\mathbf{R}_{\text{D}}^{-1}$ to decrease computation time. The resulting algorithm is summarized in Table 2.

C. Incorporating BIC

Sparsity can be incorporated by following the methodology described in the negligible Doppler case in Section II-C. The criterion in (24) can be rewritten for the revised signal model as:

$$\text{BIC}_{(\tilde{p},\tilde{k},\tilde{h})}(\eta) = 2N(L+P-1) \\ \times \ln \left[\left\| \mathbf{z} - \sum_{(p,k,h)\in\{J(\eta)\bigcup(\tilde{p},\tilde{k},\tilde{h})\}} \mathbf{y}_{p,k,h} \hat{\alpha}_{p,k,h} \right\|_2^2 \right] \\ + 5\eta \ln(2N(L+P-1)). \quad (39)$$

TABLE II
IAA FOR ANGLE-RANGE-DOPPLER IMAGING WITH A MIMO ARRAY.

initialize

$$\hat{\alpha}_{p,k,h} = \frac{\mathbf{y}_{p,k,h}^* \mathbf{z}}{\mathbf{y}_{p,k,h}^* \mathbf{y}_{p,k,h}} \ , \quad p = 1, \ldots, P \\ k = 1, \ldots, K, \ \ h = 1, \ldots, H$$

repeat

$$\mathbf{R}_{\text{D}} = \sum_{p=1}^{P} \sum_{k=1}^{K} \sum_{h=1}^{H} |\hat{\alpha}_{p,k,h}|^2 \mathbf{y}_{p,k,h} \mathbf{y}_{p,k,h}^*$$

$$\hat{\alpha}_{p,k,h} = \frac{\mathbf{y}_{p,k,h}^* \mathbf{R}_{\text{D}}^{-1} \mathbf{z}}{\mathbf{y}_{p,k,h}^* \mathbf{R}_{\text{D}}^{-1} \mathbf{y}_{p,k,h}}, \quad p = 1, \ldots, P, \\ k = 1, \ldots, K, \ \ h = 1, \ldots, H$$

until (a certain number of iterations is reached)

The peak selection procedure is identical to the one described in Section II-C with the only difference being the inclusion of the Doppler dimension in the analysis. We use 5 in the penalty term of (39) to account for the unknown target parameters: amplitude (complex valued), range, angle, and Doppler.

IV. REGULARIZED IAA (IAA-R)

In practice, a radar system may illuminate only a restricted angular region (for example, -30° to 30°) relative to the radar by adjusting the transmit beampattern of each transmit antenna. Then the scanning grid does not need to cover the entire region (-90° to 90°), and it could be limited to the angular region of interest (-30° through 30°, for example) only. Even though the reflected power at locations not corresponding to illuminated targets is small, these estimates still contribute to the rank of the covariance matrix used in IAA. As the size of the scanning grid, K, decreases, the condition number of $\mathbf{R}$ in (18) and $\mathbf{R}_{\text{D}}$ in (35) could increase to unfavorable levels. In the negligible Doppler case, $\mathbf{R}$ is invertible only if $PK \geq N\tilde{N}(L+P-1)$. For the non-negligible Doppler case, invertibility of $\mathbf{R}_{\text{D}}$ requires that $PKH \geq N(L+P-1)$. Moreover, $\mathbf{R}$ in (18) and $\mathbf{R}_{\text{D}}$ in (35) do not explicitly consider the contribution of the noise terms $\mathbf{e}$ and $\mathbf{e}_{\text{D}}$, respectively. To resolve these issues, we regularize the $\mathbf{R}$ and $\mathbf{R}_{\text{D}}$ with diagonal matrices $\mathbf{\Sigma}$ and $\mathbf{\Sigma}_{\text{D}}$, respectively, whose diagonal elements represent the unknown noise powers and are computed automatically. The regularized IAA approach, referred to hereafter as IAA-R, fits naturally within the user parameter-free framework of the existing IAA algorithm.

When intra-pulse Doppler effects are neglected, we can write the regularized version of (18) as:

$$\mathbf{R} = \sum_{p=1}^{P} \sum_{k=1}^{K} |\alpha_{p,k}|^2 \mathbf{y}_{p,k} \mathbf{y}_{p,k}^* + \mathbf{\Sigma} \ , \quad (40)$$

where the noise power estimates along the diagonal of $\mathbf{\Sigma}$ are denoted by $\{\sigma_l^2\}_{l=1}^{N\tilde{N}(L+P-1)}$. IAA-R is implemented as in Table 1, except that the number of unknowns is now increased to $KP + N\tilde{N}(L+P-1)$ from KP. The "steering vector" corresponding to σ_l is the l^{th} column of $\mathbf{I}_{N\tilde{N}(L+P-1)}$, which we denote as $\mathbf{v}_l$. Consequently, the update estimate for σ_l is

given by:

$$\hat{\sigma}_l^2 = \left| \frac{\mathbf{v}_l^* \mathbf{R}^{-1} \mathbf{d}}{\mathbf{v}_l^* \mathbf{R}^{-1} \mathbf{v}_l} \right|^2 , \quad l = 1, \ldots, N\tilde{N}(L+P-1). \quad (41)$$

The noise power estimates can be initialized as all zeros or as a small (relative to the strength of the targets) constant number.

In the non-negligible Doppler case, very similarly, we can write the regularized version of (35) as:

$$\mathbf{R}_{\mathrm{D}} = \sum_{p=1}^{P} \sum_{k=1}^{K} \sum_{h=1}^{H} |\alpha_{p,k,h}|^2 \mathbf{y}_{p,k,h} \mathbf{y}_{p,k,h}^* + \mathbf{\Sigma}_{\mathrm{D}} , \quad (42)$$

where the noise power estimates, $\{\bar{\sigma}_l^2\}_{l=1}^{N(L+P-1)}$, are again contained along the diagonal of $\mathbf{\Sigma}_{\mathrm{D}}$. The IAA-R estimate for $\bar{\sigma}_l$ is then:

$$\hat{\bar{\sigma}}_l^2 = \left| \frac{\bar{\mathbf{v}}_l^* \mathbf{R}_{\mathrm{D}}^{-1} \mathbf{z}}{\bar{\mathbf{v}}_l^* \mathbf{R}_{\mathrm{D}}^{-1} \bar{\mathbf{v}}_l} \right|^2 , \quad l = 1, \ldots, N(L+P-1), \quad (43)$$

where $\bar{\mathbf{v}}_l$ denotes the l^{th} column of $\mathbf{I}_{N(L+P-1)}$.

IAA-R performs well with irregularly sampled scanning grids and with arbitrary sensor spacings, whereas the inversion of $\mathbf{R}$ in (18) and $\mathbf{R}_{\mathrm{D}}$ in (35) without the regularizing term might be problematic in such cases. Certainly, the technique could be similarly applied to other active and passive sensing applications considered in [22] if desired.

V. Maximum Likelihood based IAA-R (IAA-R-ML)

In the previous sections, we developed an extension to the IAA algorithm which used a deterministic model for the signal of interest. We now adopt a stochastic interpretation of the signal model and use maximum likelihood (ML) techniques to estimate the target parameters. Again performing regularization on the covariance matrix, we identify this approach as IAA-R-ML. Like IAA-R, IAA-R-ML is non-parametric and user parameter-free. For conciseness, we formulate the algorithm for the non-negligible Doppler case, as the negligible Doppler version of the algorithm can be similarly synthesized.

We assume the received signal, $\mathbf{z}$, to have a complex multivariate Gaussian distribution with zero mean and covariance matrix, $\mathbf{R}_{\mathrm{D}}$, given in (35), so that the likelihood of $\mathbf{z}$ has the form:

$$p(\mathbf{z}|\mathbf{R}_{\mathrm{D}}) = \frac{1}{\pi^{N(L+P-1)}|\mathbf{R}_{\mathrm{D}}|} e^{-\mathbf{z}^* \mathbf{R}_{\mathrm{D}}^{-1} \mathbf{z}} . \quad (44)$$

Maximization of the logarithm of the likelihood with respect to the unknown terms in $\mathbf{R}_{\mathrm{D}}$ is equivalent to minimization of the following cost function:

$$\mathbf{z}^* \mathbf{R}_{\mathrm{D}}^{-1} \mathbf{z} + \ln|\mathbf{R}_{\mathrm{D}}| . \quad (45)$$

Using the matrix inversion lemma, the relationship in (36), and the properties of the determinant operation (specifically, that $|\mathbf{I} + \mathbf{AB}| = |\mathbf{I} + \mathbf{BA}|$), we obtain:

$$|\mathbf{R}_{\mathrm{D}}| = |\mathbf{Q}_{p,k,h}|(1 + |\alpha_{p,k,h}|^2 \mathbf{y}_{p,k,h}^* \mathbf{Q}_{p,k,h}^{-1} \mathbf{y}_{p,k,h}) , \quad (46)$$

and

$$\mathbf{R}_{\mathrm{D}}^{-1} = \mathbf{Q}_{p,k,h}^{-1} - \frac{|\alpha_{p,k,h}|^2 \mathbf{Q}_{p,k,h}^{-1} \mathbf{y}_{p,k,h} \mathbf{y}_{p,k,h}^* \mathbf{Q}_{p,k,h}^{-1}}{1 + |\alpha_{p,k,h}|^2 \mathbf{y}_{p,k,h}^* \mathbf{Q}_{p,k,h}^{-1} \mathbf{y}_{p,k,h}} , \quad (47)$$

where (p, k, h) represents any target of interest. For notational convenience, let $\beta_{p,k,h} = |\alpha_{p,k,h}|^2$. By using (46) and (47), the minimization of (45) with respect to $\beta_{p,k,h}$ (for fixed $\mathbf{Q}_{p,k,h}$) becomes equivalent to minimizing:

$$f(\beta_{p,k,h}) = \ln(1 + \beta_{p,k,h} \mathbf{y}_{p,k,h}^* \mathbf{Q}_{p,k,h}^{-1} \mathbf{y}_{p,k,h}) - \frac{\beta_{p,k,h} \mathbf{z}^* \mathbf{Q}_{p,k,h}^{-1} \mathbf{y}_{p,k,h} \mathbf{y}_{p,k,h}^* \mathbf{Q}_{p,k,h}^{-1} \mathbf{z}}{1 + \beta_{p,k,h} \mathbf{y}_{p,k,h}^* \mathbf{Q}_{p,k,h}^{-1} \mathbf{y}_{p,k,h}} . \quad (48)$$

To minimize (48), we set the first derivative of (48) with respect to $\beta_{p,k,h}$ to zero and solve for $\beta_{p,k,h}$:

$$\tilde{\beta}_{p,k,h} = \frac{\mathbf{y}_{p,k,h}^* \mathbf{Q}_{p,k,h}^{-1} (\mathbf{z}\mathbf{z}^* - \mathbf{Q}_{p,k,h}) \mathbf{Q}_{p,k,h}^{-1} \mathbf{y}_{p,k,h}}{(\mathbf{y}_{p,k,h}^* \mathbf{Q}_{p,k,h}^{-1} \mathbf{y}_{p,k,h})^2} . \quad (49)$$

Taking the second derivative of (48) and inserting the above estimate of $\beta_{p,k,h}$, we find that

$$f''(\tilde{\beta}_{p,k,h}) = \frac{(\mathbf{y}_{p,k,h}^* \mathbf{Q}_{p,k,h}^{-1} \mathbf{y}_{p,k,h})^2}{(1 + \tilde{\beta}_{p,k,h} \mathbf{y}_{p,k,h}^* \mathbf{Q}_{p,k,h}^{-1} \mathbf{y}_{p,k,h})^2} , \quad (50)$$

which is strictly positive. Hence, the estimate of $\beta_{p,k,h}$ in (49) is the global minimizer of (48). Though unlikely, it is possible that the estimate for $\beta_{p,k,h}$ given in (49) could be negative. To enforce nonnegativity of the power estimates, the IAA-R-ML estimate is then given by:

$$\hat{\beta}_{p,k,h} = \max\left(0, \quad \tilde{\beta}_{p,k,h} \right) . \quad (51)$$

Since $\tilde{\beta}_{p,k,h}$ is the unique minimizer of $f(\beta_{p,k,h})$ and since the first derivative of $f(\beta_{p,k,h})$ is greater than zero for $\beta_{p,k,h} > \tilde{\beta}_{p,k,h}$, we can conclude that $\hat{\beta}_{p,k,h}$ minimizes $f(\beta_{p,k,h})$ subject to $\beta_{p,k,h} \geq 0$.

As we did in the previous sections, we replace $\mathbf{Q}_{p,k,h}^{-1}$ in (49) and (51) with $\mathbf{R}_{\mathrm{D}}^{-1}$ via the matrix inversion lemma (to reduce computation):

$$\hat{\beta}_{p,k,h} = \max\left(0, \frac{\mathbf{y}_{p,k,h}^* \mathbf{R}_{\mathrm{D}}^{-1} (\mathbf{z}\mathbf{z}^* - \mathbf{R}_{\mathrm{D}}) \mathbf{R}_{\mathrm{D}}^{-1} \mathbf{y}_{p,k,h}}{(\mathbf{y}_{p,k,h}^* \mathbf{R}_{\mathrm{D}}^{-1} \mathbf{y}_{p,k,h})^2} + \beta_{p,k,h} \right) . \quad (52)$$

Since this estimate depends on $\mathbf{R}_{\mathrm{D}}$ and $\beta_{p,k,h} = |\alpha_{p,k,h}|^2$, we must again adopt an iterative approach; $\{\alpha_{p,k,h}\}$ can be initialized using DAS. Furthermore, we recalculate $\mathbf{R}_{\mathrm{D}}$ after each $\alpha_{p,k,h}$ is updated.

We can rewrite the estimate in (52) as:

$$\hat{\beta}_{p,k,h} = \max\left(0, \quad \frac{\mathbf{y}_{p,k,h}^* \mathbf{R}_{\mathrm{D}}^{-1} (\mathbf{z}\mathbf{z}^*) \mathbf{R}_{\mathrm{D}}^{-1} \mathbf{y}_{p,k,h}}{(\mathbf{y}_{p,k,h}^* \mathbf{R}_{\mathrm{D}}^{-1} \mathbf{y}_{p,k,h})^2} + \beta_{p,k,h} - \frac{1}{\mathbf{y}_{p,k,h}^* \mathbf{R}_{\mathrm{D}}^{-1} \mathbf{y}_{p,k,h}} \right) . \quad (53)$$

The term on the far right of (53) is just the estimate for $\beta_{p,k,h}$ attained with a standard Capon beamformer (SCB) [29] (assuming $\mathbf{R}_{\mathrm{D}}$ is invertible). If $\beta_{p,k,h}$ is close to the SCB estimate (which should be the case at least locally around the true values), then the estimate given in (53) is approximately

equal to the IAA-R estimate. In this way, we may view IAA-R as an approximation to IAA-R-ML.

IAA-R-ML is a cyclic algorithm that maximizes the log-likelihood function, and is therefore locally convergent. Since IAA-R is an approximation to IAA-R-ML, we expect that it shares similar convergence properties. A local convergence analysis for IAA-R, like the one for IAA presented in the appendix, is not possible since IAA-R takes into account the noise covariance matrix, whereas the analysis in the appendix is concerned with the convergence to the true parameters in the noise-free case.

VI. Numerical Results

This section uses numerical examples to demonstrate the superior performance of IAA-R over that of conventional DAS and of several adaptive beamforming algorithms as well as of the extended IAA algorithm without regularization. The advantage of a MIMO radar over a SIMO radar will also be illustrated. The MIMO radar under consideration contains $M = 5$ transmit antennas spaced at $d_t = 2.5\lambda_0$ and $N = 5$ receive antennas spaced at $d_r = 0.5\lambda_0$. In this way, i.e., with a sparse transmit array and filled receive array, we effectively create a filled virtual array with $NM = 25$ antennas [10], [11], [18]. The SIMO system under consideration, on the other hand, contains $N = 5$ receive antennas spaced at $d_r = 0.5\lambda_0$ and $M = 1$ transmit antenna. The total transmitted power of the MIMO radar is the same as that of the SIMO system.

For each of the figures shown in these examples, we fix the amplitude scale used to represent the targets; we perform thresholding to the targets that fall outside of these boundaries. In this way, we are able to accurately compare and illustrate the sidelobe levels that result from the different estimation approaches.

A. MIMO SAR Imaging with Negligible Doppler

A MIMO array for spotlight SAR imaging in the negligible intra-pulse Doppler case is considered. In other words, we assume that the scene of interest is stationary and that the radar platform is moving; we neglect the intra-pulse Doppler shifts that result from the radar's motion (as done most often in practice [31], [32]). If the motion of the radar cannot be neglected, then we could adjust the signal model to account for the radar's velocity. The true response consists of 29 targets spread randomly across $P = 24$ range bins with at least 2° separation between target scatterers. The amplitudes of the targets are selected independently from a uniform distribution on the unit interval $[0, 1]$. We provide the true target image in Figure 1(a). The angular interval of interest ranges from -30° to 30°, with 1° angular grid size, i.e., $K = 61$. We will assume circularly symmetric independent and identically distributed (i.i.d.) additive complex Gaussian noise with zero-mean and variance σ^2. We let d_n, the separation between collection positions, be $12.5\lambda_0$.

1) Example 1: For the first example, we restrict the number of data collection positions, $\tilde{N}$, to one and the length of the transmit waveform is fixed at $L = 64$. The signal-to-noise ratio (SNR), which is defined as $10\log_{10}\left(\frac{\mathrm{tr}(\mathbf{X}^*\mathbf{X})}{L\sigma^2}\right)$, is set at 20 dB.

Figures 2(a)-(b) demonstrate the performance of DAS and IAA-R with a SIMO radar. In Figure 2(a), a widely used pseudo-noise (PN) sequence [33], which has reasonably good auto-correlation properties, is transmitted and the target parameters are estimated at the receiver using DAS. The same PN sequence is transmitted for the case in Figure 2(b), but now IAA-R is used for estimating the target parameters instead of DAS. The results obtained using a MIMO radar are shown in Figures 2(c)-(e). For each of these examples, orthogonal Hadamard waveforms, scrambled with a PN sequence to improve the waveforms' merit factors, are transmitted [33]. In Figures 2(c)-(d), DAS and IAA-R, respectively, are used to estimate the target parameters. The IAA-R estimate when the BIC algorithm is applied is shown in Figure 2(e).

From Figure 2, we observe that the MIMO system offers much improved resolution over the SIMO system, even when using DAS as the receive filter. On the other hand, it is observed that IAA-R successfully refines the DAS estimates in both the SIMO and MIMO cases to effectively reduce the sidelobe levels. IAA-R shows quite good estimation accuracy in the MIMO case. To evaluate the performance of IAA-R with BIC for the SIMO and MIMO systems, we compare the probability of detection (P_D) and the probability of false alarm (P_{FA}) for each case; we let P_D = (number of targets detected) / (total number of true targets) and P_{FA} = (total number of false positives) / (total number of grid points not occupied by targets). We classify a target as successfully identified if BIC chooses a point within 1° of the true target location (and within the same range bin). For the SIMO result in Figure 2(c), $P_D = 65.5\%$ and $P_{FA} = 1.0\%$. For the MIMO result in Figure 2(f), $P_D = 96.6\%$ and $P_{FA} = 0\%$. As BIC does not provide satisfactory results for the IAA-R result from the SIMO system, we ommit these images in the next examples. We furthermore neglect to show the results of applying BIC to the DAS results, as the poor resolution of these images, with BIC applied, would lead to an unacceptably low P_D [25].

In Figure 3, we show the results of using IAA without regularization for the MIMO case. For Figure 3(a), the radar scans an angular interval of interest ranging from -30° to 30°, with 1° angular grid size, as in the previous images. Since, in this case, the condition number of $\mathbf{R}$ in (18) reaches unfavorable levels (due to K being small relative to the entire angular region), IAA suffers from poor performance. In Figure 3(b), on the other hand, the scanning region is increased to -90° through 90° (the entire scanning region), again with 1° angular grid size. In this image, however, only the angular region of interest (-30° to 30°) is shown. The condition number of $\mathbf{R}$ in (18) is significantly reduced in this case (since K is much larger), and the performance of IAA improves drastically. Thus, we conclude that IAA works well when the entire angular region is considered. If the targets are known to exist within a smaller region relative to the whole scanning grid, then the actual scanning grid can be decreased to reduce computational costs by using IAA-R instead to avoid problems that might arise with the inversion of $\mathbf{R}$.

2) Example 2: In the second example, we consider the performance of IAA-R when the noise level is raised. We restrict our attention to the MIMO array due to its better performance in the previous example compared to a SIMO system. For this example, the SNR was set at 15 dB, $L = 32$, and $\tilde{N} = 3$. We again transmit orthogonal Hadamard waveforms scrambled with a PN sequence.

Figures 4(a)-(c) show the DAS, Capon, and APES estimates of the scene, respectively. To form a MIMO radar image using these techniques, we first form a synthetic aperture using the returns from the $\tilde{N}$ positions, and then perform range compression to form the matrix $\tilde{\mathbf{D}}_p$:

$$\tilde{\mathbf{D}}_p = \left[\begin{array}{cccc} \mathbf{D}_p^*(1)\mathbf{Y}_{\text{MF}}, & \mathbf{D}_p^*(2)\mathbf{Y}_{\text{MF}}, & \ldots, & \mathbf{D}_p^*(\tilde{N})\mathbf{Y}_{\text{MF}} \end{array} \right], \quad p = 1, \ldots, P, \quad (54)$$

where $\mathbf{Y}_{\text{MF}}$ represents the matched filter ($\mathbf{Y}_{\text{MF}} = \mathbf{X}(\mathbf{X}^*\mathbf{X})^{-1}$) and $\mathbf{D}_p^*(n) \in \mathbb{C}^{N \times L}$ denotes the portion of the received signal (from position n) synchronized with the return from the pth range bin. We can then apply Capon or APES to $\tilde{\mathbf{D}}_p$ to obtain an estimate for targets at the pth range bin [19], [34]. Data-adaptive methods, such as Capon and APES, perform poorly when the number of data snapshots, which is represented by the number of columns in (54) (for this example, $M\tilde{N} = 15$), is not significantly greater than the number of array sensors ($N = 5$) [21]. In this case, the estimated signal covariance matrix, which depends directly on the number of data snapshots, can differ significantly from the true covariance matrix. When only a single snapshot is attained ($M = \tilde{N} = 1$ in (54)), adaptive beamforming methods fail, since the sample covariance matrix becomes singular. IAA-R (and IAA), on the other hand, can perform well even when the number of snapshots is one. For this example, we see much better results using IAA-R and IAA-R with BIC (compared to Capon and APES), as shown in Figures 4(d) and 4(e), respectively.

In Figure 4(f), a plot of the mean-squared error (MSE) of IAA-R versus the iteration number is shown, with MSE defined as:

$$\frac{\|\mathbf{B}_0 - \mathbf{B}_{\text{IAA-R}}^{(i)}\|_{\text{F}}^2}{\|\mathbf{B}_0\|_{\text{F}}^2}, \quad (55)$$

where i denotes the iteration number, $\mathbf{B}_0$ denotes the ground truth and $\mathbf{B}_{\text{IAA-R}}^{(i)}$ denotes the IAA-R range-angle image estimate at iteration i. Iteration 0 denotes the MSE of DAS (as IAA-R is initialized with DAS). Note that the MSE value decreases monotonically with the iteration number and appears to converge after only a few iterations of IAA-R.

B. MIMO Range-Angle-Doppler Imaging with Non-negligible Doppler

This subsection considers the non-negligible intra-pulse Doppler case; the antenna array (with the same structure as before) is assumed vertical and stationary, and the targets are assumed mobile. The ground truth consists of 4 targets placed within $P = 24$ range bins. We represent the Doppler shift, in degrees, of a target in a particular Doppler bin as $\Phi_h = \omega_h L(180^\circ/\pi)$, $h = 1, \ldots, H$. The Doppler interval of interest, which ranges from -90° to 90°, is divided into 181 bins resulting in 1° Doppler grid size. All of the scatterers are located at a Doppler angle of 1°, which corresponds to a target moving at approximately 40 m/s for X-band radar (a faster object, which would have a larger Doppler angle, would be easier to detect). We again let $K = 61$ and the angular interval range from -30° to 30° with 1° grid size. L is set at 32. The targets are positioned at an angle of 1° relative to the array normal. We provide the true target image in Figure 1(b). As before, i.i.d. circularly symmetric complex Gaussian noise is assumed with a 20 dB SNR. The stationary ground clutter return is 20 dB stronger than the targets and is placed at a Doppler angle of 0° and at -9° relative to the array normal. In the following examples, the dynamic range is chosen to extend from -25 dB to 25 dB and the amplitude estimates were coerced into this interval through hard limiting.

1) Example 1: The DAS and IAA-R estimates using a SIMO array and a PN transmit signal are shown in Figures 5(a)-(b). In these figures, we examine a range-Doppler slice of the target estimates taken at 1° relative to a broadside scan. The results obtained using a MIMO array are shown in Figures 5(c)-(e), using DAS, IAA-R, and IAA-R with BIC, respectively. For these images, we again transmit Hadamard waveforms scrambled with PN sequences. From the range-Doppler results, we can observe that the DAS images for both the SIMO and MIMO arrays have significantly lower resolution than the corresponding IAA-R images, and none of the targets can be identified using DAS. Furthermore, the IAA-R image obtained using a MIMO array demonstrates superior performance over that obtained using a SIMO array; the IAA-R with BIC algorithm produces a sparse result and identifies all of the targets in the scene.

2) Example 2: In the second example, the angle-range slice (chosen at a certain Doppler shift) of the estimated target parameters is considered. Particularly, the slice corresponding to the 1° Doppler bin, which corresponds to the Doppler shift of our target responses, is selected. For each image shown, the transmit waveforms used correspond to their respective images shown in Figure 5. The DAS and IAA-R results with a SIMO array are shown in Figures 6(a)-(b), respectively. For the MIMO radar case, the DAS and IAA-R results are shown in Figures 6(c)-(d), respectively. Due to the strong presence of the ground return in this angle-range slice, the BIC result was not satisfactory and thus the result is not shown. As evidenced, the poor resolution and accuracy of DAS is further emphasized from the angle-range perspective. In addition, the improved angular resolution that results from using the MIMO array, as compared to the SIMO antenna array, is demonstrated in the IAA-R result. The IAA-R result again shows notably better performance than DAS.

In Figures 6(a) and 6(c), a null (approximately zero amplitude) occurs in the amplitude estimates at 14°, across all range bins. When we apply a DAS receive filter matched to 14°, a zero occurs in the filter response at precisely -9°. Thus, the contribution from the clutter ground return is removed from target estimates at 14°. In Figure 6(e), we show the beampattern response of the DAS filter, which is steered to 14°. As evidenced, the ground clutter return offers no

contribution to these target estimates.

C. Complexity Analysis

The per iteration computational complexity of IAA-R in the negligible and non-negligible Doppler cases is $\mathcal{O}((N\tilde{N}(L+P-1))^2(PK))$ and $\mathcal{O}((N(L+P-1))^2(PKH))$, respectively, whereas the total complexity of DAS is $\mathcal{O}(N\tilde{N}(L+P-1)(PK))$ and $\mathcal{O}(N(L+P-1)(PKH))$ for the negligible and non-negligible Doppler cases, respectively. The superior performance of IAA-R over all the other considered methods justifies its increased computational cost, especially in view of the fact that IAA-R can be used to update all grid points of interest and noise variances in parallel in each iteration.

VII. Conclusions

In this paper, we have presented a user parameter-free and non-parametric iterative adaptive approach, namely IAA, for MIMO radar imaging applications with both negligible intra-pulse Doppler (e.g., spotlight SAR stationary target imaging) and with non-negligible intra-pulse Doppler (mobile target imaging). We further provided a local convergence analysis of IAA. A regularized version of IAA, IAA-R, was proposed in order to improve the performance of IAA and to make it work with incomplete scanning regions, which is usually the case in radar applications. Compared to a SIMO phased-array radar, application of a MIMO radar system resulted in higher angular resolution as well as higher Doppler resolution. Furthermore, IAA-R demonstrated superior performance for both array systems, as compared to DAS, adaptive beamforming techniques, and the IAA algorithm with incomplete scanning regions and without regularization. By incorporating the BIC algorithm, we were able to produce further sparsity in the IAA-R result. Finally, we also derived the maximum likelihood based IAA-R-ML, which assumes a statistical model on the received signal and is guaranteed to be locally convergent. We showed how IAA-R can be viewed as an approximation to IAA-R-ML.

Appendix
Local Convergence Analysis of IAA

Consider a generic data model, similar to the one in (13):

$$\mathbf{d} = \mathbf{A}\boldsymbol{\alpha} + \mathbf{e}\,, \tag{56}$$

where $\mathbf{d} \in \mathbb{C}^{\bar{M}\times 1}$, $\mathbf{A} \in \mathbb{C}^{\bar{M}\times\bar{N}}$ ($\bar{N} > \bar{M}$), $\boldsymbol{\alpha} \in \mathbb{C}^{\bar{N}\times 1}$, $\mathbf{e} \in \mathbb{C}^{\bar{M}\times 1}$, and

$$\mathbf{A} = \left[\begin{array}{ccc} \mathbf{a}_1 & \dots & \mathbf{a}_{\bar{N}} \end{array}\right]. \tag{57}$$

The analysis below assumes that $\mathbf{e}$ is negligible. In the absence of noise, $\mathbf{d}$ is assumed to have the form:

$$\mathbf{d} = \tilde{\mathbf{A}}\tilde{\boldsymbol{\alpha}}\,, \tag{58}$$

where $\tilde{\mathbf{A}} \in \mathbb{C}^{\bar{M}\times\bar{K}}$, ($\bar{K} < \bar{M}$), rank$(\tilde{\mathbf{A}}) = \bar{K}$, and

$$\tilde{\boldsymbol{\alpha}} = \left[\begin{array}{ccc} \tilde{\alpha}_1 & \dots & \tilde{\alpha}_{\bar{K}} \end{array}\right]^T, \tag{59}$$

with $\tilde{\alpha}_k \neq 0\ \forall k$. Let

$$\tilde{\mathbf{A}} = \left[\begin{array}{ccc} \tilde{\mathbf{a}}_1 & \dots & \tilde{\mathbf{a}}_{\bar{K}} \end{array}\right]. \tag{60}$$

We assume that there exist $n_1, \dots, n_{\bar{K}}$ such that $\tilde{\mathbf{a}}_k = \mathbf{a}_{n_k}$, $k = 1, \dots, \bar{K}$. Also, we assume that the columns of $\mathbf{A}$ that are different from those of $\tilde{\mathbf{A}}$ do not belong to the range space of $\tilde{\mathbf{A}}$, i.e., $\mathbf{a}_n \notin$ Range$(\tilde{\mathbf{A}})$ for $n \neq n_k$, $k = 1, \dots, \bar{K}$. These assumptions are typical of the sparse estimation approaches [35].

Consider the following regularized IAA algorithm (to avoid numerical ill-conditioning, see below for details). Let (similarly to (18))

$$\mathbf{R} = \mathbf{A}\mathbf{P}\mathbf{A}^* + \rho\mathbf{I}\,, \tag{61}$$

where $\rho > 0$ is a small scalar and

$$\mathbf{P} = \left[\begin{array}{ccc} |\alpha_1|^2 & & 0 \\ & \ddots & \\ 0 & & |\alpha_{\bar{N}}|^2 \end{array}\right]. \tag{62}$$

Let i denote the iteration index. Then (see (20) and (21)), for $n = 1, \dots, \bar{N}$,

$$\alpha_n^{i+1} = \frac{\mathbf{a}_n^*(\mathbf{Q}_n^i)^{-1}\mathbf{d}}{\mathbf{a}_n^*(\mathbf{Q}_n^i)^{-1}\mathbf{a}_n}\,, \tag{63}$$

and

$$\begin{array}{rcl} \mathbf{Q}_n^i & = & \sum_{k=1,k\neq n}^{\bar{N}} |\alpha_k^i|^2\mathbf{a}_k\mathbf{a}_k^* + \rho\mathbf{I} \\ & = & \mathbf{R}^i - |\alpha_n^i|^2\mathbf{a}_n\mathbf{a}_n^*\,. \end{array} \tag{64}$$

Remarks: (a) The regularization parameter ρ in (61) can be chosen only slightly larger than the value needed to avoid an ill-conditioning message during the numerical implementation. In practical applications, one may choose $\rho = 0$ first until the ill-conditioning warning occurs, at which point one may replace the $\rho = 0$ with a small $\rho > 0$. (b) Using the matrix inversion lemma, we can show that $(\mathbf{Q}_n^i)^{-1}$ in IAA can be replaced by $(\mathbf{R}^i)^{-1}$ (see (22) and (23)). However, as suggested by the calculations below, the computational advantage that follows from this replacement is offset by the fact that, close to convergence, the use of $(\mathbf{Q}_n^i)^{-1}$ in IAA turns out to lead to a numerically more stable algorithm. In practical applications, one may use $(\mathbf{R}^i)^{-1}$ at the beginning of the iterations until the first ill-conditioning warning occurs, at which point one may replace $(\mathbf{R}^i)^{-1}$ with $\rho(\mathbf{Q}_n^i)^{-1}$ (see (71) below). □

Consider first the stationary points of IAA. These points satisfy the equation:

$$\alpha_n = \frac{\mathbf{a}_n^*\mathbf{Q}_n^{-1}\mathbf{d}}{\mathbf{a}_n^*\mathbf{Q}_n^{-1}\mathbf{a}_n}\,, \quad n = 1, \dots, \bar{N}\,. \tag{65}$$

Note first that $\alpha_n = 0$, $n = 1, \dots, \bar{N}$, is not one of the stationary points. To see this, note that setting $\alpha_n = 0$ in the right hand side of (65) yields

$$\alpha_n = \frac{\mathbf{a}_n^*\mathbf{d}}{\|\mathbf{a}_n\|^2} = 0\,, \quad n = 1, \dots, \bar{N}\,, \tag{66}$$

which is generally a contradiction. This result starkly contrasts what happens for most sparse algorithms (such as FOCUSS, etc.), for which $\alpha_n = 0$ is a stationary point [35]. More importantly, we note that the true $\tilde{\boldsymbol{\alpha}}$ gives a stationary point (as $\rho \to 0$), i.e.,

$$\alpha_n = \left\{\begin{array}{ll} \tilde{\alpha}_k\,, & n = n_k\,,\ k = 1, \dots, \bar{K} \\ 0\,, & n \neq n_k\,,\ k = 1, \dots, \bar{K}\,. \end{array}\right. \tag{67}$$

To see this, first observe that the matrices $\mathbf{Q}_n$ corresponding to (67) are given by:

$$\mathbf{Q}_n = \begin{cases} \tilde{\mathbf{A}}_k \tilde{\mathbf{P}}_k \tilde{\mathbf{A}}_k^* + \rho \mathbf{I}\,, & n = n_k\,,\ k = 1, \ldots, \bar{K} \\ \tilde{\mathbf{A}} \tilde{\mathbf{P}} \tilde{\mathbf{A}}^* + \rho \mathbf{I}\,, & n \neq n_k\,,\ k = 1, \ldots, \bar{K}\,, \end{cases} \tag{68}$$

where $\tilde{\mathbf{A}}_k$ is the matrix $\tilde{\mathbf{A}}$ without the kth column,

$$\tilde{\mathbf{P}} = \begin{bmatrix} |\tilde{\alpha}_1|^2 & & 0 \\ & \ddots & \\ 0 & & |\tilde{\alpha}_{\bar{K}}|^2 \end{bmatrix}, \tag{69}$$

and $\tilde{\mathbf{P}}_k$ is the above matrix without the kth row and column.

Next, let us consider a general matrix having the form of (68):

$$\mathbf{Q} = \mathbf{B}\mathbf{B}^* + \rho \mathbf{I}\,, \tag{70}$$

where $\mathbf{B}^*\mathbf{B} > 0$. For $\rho \to 0$, we have that

$$\begin{array}{rcl} \rho \mathbf{Q}^{-1} & = & \mathbf{I} - \frac{1}{\rho}\mathbf{B}(\mathbf{I} + \frac{1}{\rho}\mathbf{B}^*\mathbf{B})^{-1}\mathbf{B}^* \\ & = & \mathbf{I} - \mathbf{B}(\rho \mathbf{I} + \mathbf{B}^*\mathbf{B})^{-1}\mathbf{B}^* \\ & \xrightarrow{\rho \to 0} & \mathbf{I} - \mathbf{B}(\mathbf{B}^*\mathbf{B})^{-1}\mathbf{B}^* = \mathbf{P}_{\mathbf{B}}^{\perp}\,, \end{array} \tag{71}$$

where $\mathbf{P}_{\mathbf{B}}^{\perp}$ is the orthogonal projector onto the null space of $\mathbf{B}^*$.

It follows from (68) and (71), as well as the assumptions made, that (for ρ tending to zero):

$$\alpha_n = \begin{cases} \frac{\mathbf{a}_{n_k}^* \mathbf{P}_{\tilde{\mathbf{A}}_k}^{\perp} \tilde{\mathbf{A}} \tilde{\boldsymbol{\alpha}}}{\mathbf{a}_{n_k}^* \mathbf{P}_{\tilde{\mathbf{A}}_k}^{\perp} \mathbf{a}_{n_k}} = \tilde{\alpha}_k\,, & n = n_k\,,\ k = 1, \ldots, \bar{K} \\ \frac{\mathbf{a}_n^* \mathbf{P}_{\tilde{\mathbf{A}}}^{\perp} \tilde{\mathbf{A}} \tilde{\boldsymbol{\alpha}}}{\mathbf{a}_n^* \mathbf{P}_{\tilde{\mathbf{A}}}^{\perp} \mathbf{a}_n} = 0\,, & n \neq n_k\,,\ k = 1, \ldots, \bar{K}\,. \end{cases} \tag{72}$$

Note that $\mathbf{a}_{n_k}^* \mathbf{P}_{\tilde{\mathbf{A}}_k}^{\perp} \mathbf{a}_{n_k} \neq 0$ because $\mathbf{a}_{n_k} \notin \text{Range}(\tilde{\mathbf{A}}_k)$, and similarly for $\mathbf{a}_n^* \mathbf{P}_{\tilde{\mathbf{A}}}^{\perp} \mathbf{a}_n$. With these observations, the proof that (67) is a stationary point of IAA (for $\rho \to 0$) is concluded.

Remark: If we replaced $\mathbf{Q}_n$ with $\mathbf{R}$ in the IAA algorithm, then the denominator in the first equation of (72) would have been $\mathbf{a}_{n_k}^* \mathbf{P}_{\tilde{\mathbf{A}}}^{\perp} \mathbf{a}_{n_k} = 0$, which points to the ill-conditioning that might be caused by such a replacement as briefly mentioned in Remark (b) following (64). □

Next, we prove the local convergence of IAA to the true values. Let us denote the true values in (67) by $\{\alpha_n^0\}$:

$$\alpha_n^0 = \begin{cases} \tilde{\alpha}_k\,, & n = n_k\,,\ k = 1, \ldots, \bar{K} \\ 0\,, & n \neq n_k\,,\ k = 1, \ldots, \bar{K}\,. \end{cases} \tag{73}$$

Assume that IAA is initialized as follows:

$$\alpha_n = \begin{cases} c_k\,, & n = n_k\,,\ k = 1, \ldots, \bar{K} \\ O(\epsilon)\,, & n \neq n_k\,,\ k = 1, \ldots, \bar{K}\,, \end{cases} \tag{74}$$

where $O(\epsilon)$ denotes a term that tends to zero as ϵ, when $\epsilon \to 0$, and $\{c_k\}$ are arbitrary non-zero constants. Also, assume that the regularization parameter is given by $\rho = \epsilon^2$. We will show, under these assumptions, that one step of IAA yields, for ϵ approaching zero:

$$\hat{\alpha}_n = \alpha_n^0 + O(\epsilon^2)\,, \tag{75}$$

which implies that *IAA is locally convergent with at least a quadratic rate* (note that the attribute "local" here refers to the initialization of the zero components of $\{\alpha_n^0\}$; the non-zero components of this vector can be initialized arbitrarily!) .

To prove (75), first observe from (74) that:

$$|\alpha_n|^2 = \ O(\epsilon^2), \qquad n \neq n_k\,,\ k = 1, \ldots, \bar{K}\ . \tag{76}$$

Let

$$\mathbf{Q}_n = \sum_{k=1, k \neq n}^{\bar{N}} |\alpha_k|^2 \mathbf{a}_k \mathbf{a}_k^* + \rho \mathbf{I}\,, \tag{77}$$

let $\mathbf{S}$ denote an orthonormal basis of Range$(\tilde{\mathbf{A}}_n)$, and let $\mathbf{G}$ comprise an orthonormal basis of the null space of $\tilde{\mathbf{A}}_n^*$. (We omit the dependence of $\mathbf{S}$ and $\mathbf{G}$ on n to simplify the notation.) Using this notation, we can write (under the assumptions made):

$$\mathbf{Q}_n = \tilde{\mathbf{A}}_n \mathbf{C} \tilde{\mathbf{A}}_n^* + \mathbf{B}_n \mathbf{D} \mathbf{B}_n^* + \epsilon^2 \mathbf{I}\,, \tag{78}$$

where $\tilde{\mathbf{A}}_n = \tilde{\mathbf{A}}$ for $n \neq n_k$ ($k = 1, \cdots, \bar{K}$) by convention, $\mathbf{B}_n$ is the matrix whose columns are equal to the vectors $\{\mathbf{a}_k\}_{k \neq n}$ in (77) that do not appear in $\tilde{\mathbf{A}}$, $\mathbf{C}$ is a diagonal matrix with diagonal elements $\{c_k\}_{k=1, k \neq n}^{\bar{K}}$ corresponding to the $\{\mathbf{a}_k\}$ in $\tilde{\mathbf{A}}_n$, and $\mathbf{D}$ is a diagonal matrix made from the terms $\{|\alpha_k|^2\}$ corresponding to the $\{\mathbf{a}_k\}$ in $\mathbf{B}_n$; hence $\mathbf{D} = \mathbf{O}(\epsilon^2)$ (see (76)).

Next, we note that there exist constant matrices $\mathbf{E}$, $\mathbf{F}$ and $\mathbf{H}$ such that:

$$\tilde{\mathbf{A}}_n = \mathbf{S}\mathbf{H}\,, \tag{79}$$

and

$$\mathbf{B}_n = \begin{bmatrix} \mathbf{S} & \mathbf{G} \end{bmatrix} \begin{bmatrix} \mathbf{E} \\ \mathbf{F} \end{bmatrix}. \tag{80}$$

Inserting (79) and (80) into (78), we can rewrite the expression for $\mathbf{Q}_n$ as:

$$\begin{array}{rcl} \mathbf{Q}_n & = & \mathbf{S}\mathbf{H}\mathbf{C}\mathbf{H}^*\mathbf{S}^* + \begin{bmatrix} \mathbf{S} & \mathbf{G} \end{bmatrix} \begin{bmatrix} \mathbf{E}\mathbf{D}\mathbf{E}^* & \mathbf{E}\mathbf{D}\mathbf{F}^* \\ \mathbf{F}\mathbf{D}\mathbf{E}^* & \mathbf{F}\mathbf{D}\mathbf{F}^* \end{bmatrix} \\ & & \times \begin{bmatrix} \mathbf{S}^* \\ \mathbf{G}^* \end{bmatrix} + \epsilon^2 \begin{bmatrix} \mathbf{S} & \mathbf{G} \end{bmatrix} \begin{bmatrix} \mathbf{S}^* \\ \mathbf{G}^* \end{bmatrix} \\ & = & \begin{bmatrix} \mathbf{S} & \mathbf{G} \end{bmatrix} \begin{bmatrix} \mathbf{W}_1 & \mathbf{W}_3 \\ \mathbf{W}_3^* & \mathbf{W}_2 \end{bmatrix} \begin{bmatrix} \mathbf{S}^* \\ \mathbf{G}^* \end{bmatrix}, \end{array} \tag{81}$$

where

$$\mathbf{W}_1 = \mathbf{H}\mathbf{C}\mathbf{H}^* + \mathbf{E}\mathbf{D}\mathbf{E}^* + \epsilon^2 \mathbf{I} = \mathbf{H}\mathbf{C}\mathbf{H}^* + \mathbf{O}(\epsilon^2) \tag{82}$$

tends to a nonsingular matrix, namely $\mathbf{H}\mathbf{C}\mathbf{H}^*$, as $\epsilon \to 0$,

$$\mathbf{W}_2 = \mathbf{F}\mathbf{D}\mathbf{F}^* + \epsilon^2 \mathbf{I} = \mathbf{O}(\epsilon^2) \tag{83}$$

is a nonsingular matrix for any $\epsilon > 0$, and

$$\mathbf{W}_3 = \mathbf{E}\mathbf{D}\mathbf{F}^* = \mathbf{O}(\epsilon^2)\,. \tag{84}$$

$$\begin{bmatrix} \mathbf{W}_1 & \mathbf{W}_3 \\ \mathbf{W}_3^* & \mathbf{W}_2 \end{bmatrix}^{-1} = \begin{bmatrix} (\mathbf{W}_1 - \mathbf{W}_3\mathbf{W}_2^{-1}\mathbf{W}_3^*)^{-1} & -(\mathbf{W}_1 - \mathbf{W}_3\mathbf{W}_2^{-1}\mathbf{W}_3^*)^{-1}\mathbf{W}_3\mathbf{W}_2^{-1} \\ -\mathbf{W}_2^{-1}\mathbf{W}_3^*(\mathbf{W}_1 - \mathbf{W}_3\mathbf{W}_2^{-1}\mathbf{W}_3^*)^{-1} & (\mathbf{W}_2 - \mathbf{W}_3^*\mathbf{W}_1^{-1}\mathbf{W}_3)^{-1} \end{bmatrix}. \tag{85}$$

For any $\epsilon^2 > 0$, the inverse of the partitioned matrix in (81) exists and is given by (85) at the bottom of the previous page. Observe that the (1,1), (1,2), and (2,1) blocks of the above matrix tend to constant matrices as $\epsilon \to 0$, whereas the (2,2) block tends to infinity as $1/\epsilon^2$. It follows from this observation along with (81) and (85) that:

$$\begin{aligned} \epsilon^2 \mathbf{Q}_n^{-1} &= \left[\begin{array}{cc} \mathbf{S} & \mathbf{G} \end{array} \right] \left[\begin{array}{cc} \mathbf{O}(\epsilon^2) & \mathbf{O}(\epsilon^2) \\ \mathbf{O}(\epsilon^2) & \mathbf{\Delta} \end{array} \right] \left[\begin{array}{c} \mathbf{S}^* \\ \mathbf{G}^* \end{array} \right] \\ &= \mathbf{G}\mathbf{\Delta}\mathbf{G}^* + \mathbf{O}(\epsilon^2)\,, \end{aligned} \tag{86}$$

where

$$\begin{aligned} \mathbf{\Delta} &= \epsilon^2 (\mathbf{W}_2 - \mathbf{W}_3^* \mathbf{W}_1^{-1} \mathbf{W}_3)^{-1} \\ &= \left[\mathbf{I} + \mathbf{F} \left(\frac{1}{\epsilon^2} \mathbf{D} \right) \mathbf{F}^* \right]^{-1} + \mathbf{O}(\epsilon^2) \end{aligned} \tag{87}$$

tends to a constant positive-definite matrix as $\epsilon^2 \to 0$.

Making use of (86) in the main equation of the IAA algorithm yields:

$$\hat{\alpha}_n = \frac{\mathbf{a}_n^* \epsilon^2 \mathbf{Q}_n^{-1} \mathbf{d}}{\mathbf{a}_n^* \epsilon^2 \mathbf{Q}_n^{-1} \mathbf{a}_n} = \frac{\mathbf{a}_n^* \mathbf{G}\mathbf{\Delta}\mathbf{G}^* \mathbf{d}}{\mathbf{a}_n^* \mathbf{G}\mathbf{\Delta}\mathbf{G}^* \mathbf{a}_n} + O(\epsilon^2)\,, \tag{88}$$

from which we can obtain (75) by a calculation similar to (72). The proof of (75) is thus concluded.

In Figures 7(a)-(b), we provide an example to illustrate the convergence behavior of IAA and its dependence on ρ, as discussed above. We simulate a 1-D passive array with $N = 10$ receiving antennas separated at $d_r = 0.5\lambda_0$ and with only a single data snapshot. This antenna array scans from -90° to 90°, relative to the array normal, with 1° separation between adjacent scanning points. Two target signals, each with unit power, are located at 7° and 14°, respectively. We neglect noise in this example. In Figure 7(a), we show the DAS estimate for this case. In Figure 7(b), we show the result of IAA after 10 iterations. When applying IAA, we use $\rho = 0$ until the first ill-conditioning message for $\mathbf{R}$ occurs in MATLAB. At that point, we switch to using the minimum ρ needed to avoid ill-conditioning. For this case, we do not need ρ until the very last iteration, at which point we chose $\rho = 10^{-14}$, which was approximately the minimum value needed to avoid an error message. As shown, IAA provides a much improved result over the DAS image, which serves to illustrate the convergence analysis in this appendix.

REFERENCES

[1] E. Fishler, A. Haimovich, R. Blum, D. Chizhik, L. Cimini, and R. Valenzuela, "MIMO radar: an idea whose time has come," *Proceedings of the IEEE Radar Conference*, pp. 71–78, April 2004.

[2] E. Fishler, A. Haimovich, R. Blum, L. Cimini, D. Chizhik, and R. Valenzuela, "Performance of MIMO radar systems: advantages of angular diversity," *38th Asilomar Conference on Signals, Systems and Computers,* Pacific Grove, CA, vol. 1, pp. 305–309, November 2004.

[3] ——, "Spatial diversity in radars - models and detection performance," *IEEE Transactions on Signal Processing*, vol. 54, no. 3, pp. 823–838, March 2006.

[4] N. Lehmann, E. Fishler, A. M. Haimovich, R. S. Blum, D. Chizhik, L. Cimini, and R. Valenzuela, "Evaluation of transmit diversity in MIMO-radar direction finding," *IEEE Transactions on Signal Processing*, vol. 55, no. 5, pp. 2215–2225, May 2007.

[5] A. H. Haimovich, R. S. Blum, and L. J. Cimini, "MIMO radar with widely separated antennas," *IEEE Signal Processing Magazine*, vol. 25, no. 1, pp. 116–129, Jan 2008.

[6] I. Bekkerman and J. Tabrikian, "Spatially coded signal model for active arrays," *The 2004 IEEE International Conference on Acoustics, Speech, and Signal Processing,* Montreal, Quebec, Canada, vol. 2, pp. ii/209–ii/212, March 2004.

[7] F. C. Robey, S. Coutts, D. D. Weikle, J. C. McHarg, and K. Cuomo, "MIMO radar theory and experimental results," *38th Asilomar Conference on Signals, Systems and Computers,* Pacific Grove, CA, vol. 1, pp. 300–304, November 2004.

[8] L. B. White and P. S. Ray, "Signal design for MIMO diversity systems," *38th Asilomar Conference on Signals, Systems and Computers,* Pacific Grove, CA, vol. 1, pp. 973 – 977, November 2004.

[9] J. Li and P. Stoica, Eds., *MIMO Radar Signal Processing*. New York, NY: John Wiley & Sons, Inc., 2009.

[10] K. Forsythe, D. Bliss, and G. Fawcett, "Multiple-input multiple-output (MIMO) radar: performance issues," *38th Asilomar Conference on Signals, Systems and Computers,* Pacific Grove, CA, vol. 1, pp. 310–315, November 2004.

[11] D. W. Bliss and K. W. Forsythe, "Multiple-input multiple-output (MIMO) radar and imaging: degrees of freedom and resolution," *37th Asilomar Conference on Signals, Systems and Computers,* Pacific Grove, CA, vol. 1, pp. 54–59, November 2003.

[12] J. Li and P. Stoica, "MIMO radar with colocated antennas: Review of some recent work," *IEEE Signal Processing Magazine*, vol. 24, no. 5, pp. 106–114, September 2007.

[13] D. R. Fuhrmann and G. S. Antonio, "Transmit beamforming for MIMO radar systems using partial signal correlation," *38th Asilomar Conference on Signals, Systems and Computers,* Pacific Grove, CA, vol. 1, pp. 295–299, November 2004.

[14] D. R. Fuhrmann and G. San Antonio, "Transmit beamforming for MIMO radar systems using signal cross-correlation," *IEEE Transactions on Aerospace and Electronic Systems*, vol. 44, no. 1, pp. 1–16, January 2008.

[15] J. Li, P. Stoica, and Y. Xie, "On probing signal design for MIMO radar," *40th Asilomar Conference on Signals, Systems and Computers* (invited), Pacific Grove, CA, October 2006.

[16] P. Stoica, J. Li, and X. Zhu, "Waveform synthesis for diversity-based transmit beampattern design," *IEEE Transactions on Signal Processing*, vol. 56, no. 6, pp. 2593–2598, June 2008.

[17] P. Stoica, J. Li, and Y. Xie, "On probing signal design for MIMO radar," *IEEE Transactions on Signal Processing*, vol. 55, no. 8, pp. 4151–4161, August 2007.

[18] J. Li, P. Stoica, L. Xu, and W. Roberts, "On parameter identifiability of MIMO radar," *IEEE Signal Processing Letters*, vol. 14, no. 12, pp. 968–971, December 2007.

[19] L. Xu, J. Li, and P. Stoica, "Target detection and parameter estimation for MIMO radar systems," *IEEE Transactions on Aerospace and Electronic Systems*, vol. 44, no. 3, pp. 927–939, July 2008.

[20] J. Capon, "High resolution frequency-wavenumber spectrum analysis," *Proceedings of the IEEE*, vol. 57, pp. 1408–1418, August 1969.

[21] J. Li and P. Stoica, Eds., *Robust Adaptive Beamforming*. New York, NY: John Wiley & Sons, 2005.

[22] T. Yardibi, J. Li, P. Stoica, M. Xue, and A. B. Baggeroer, "Source localization and sensing: A nonparametric iterative adaptive approach based on weighted least squares," to appear in *IEEE Transactions on Aerospace and Electronic Systems*, available at http://www.sal.ufl.edu/eel6935/2008/IAA.pdf.

[23] W. Roberts, T. Yardibi, J. Li, X. Tan, and P. Stoica, "Sparse signal representation for MIMO radar imaging," *42nd Asilomar Conference on Signals, Systems and Computers* (invited), Pacific Grove, CA, October 2008.

[24] W. Roberts, P. Stoica., J. Li, T. Yardibi, and F. A. Sadjadi, "MIMO radar angle-range-doppler imaging," *IEEE Radar Conference,* Pasadena, CA, May 2009.

[25] P. Stoica, J. Li, and H. He, "Spectral analysis of non-uniformly sampled data: a new approach versus the periodogram," *IEEE Transactions on Signal Processing*, vol. 57, no. 3, pp. 843–858, Mar. 2009.

[26] X. Tan, W. Roberts, J. Li, and P. Stoica, "Range-Doppler imaging via a train of probing pulses," to appear *IEEE Transactions on Signal Processing*.

[27] M. I. Skolnik, *Radar Handbook*. New York, NY: McGraw-Hill Book Co., 1990.

[28] J. Li and P. Stoica, "An adaptive filtering approach to spectral estimation and SAR imaging," *IEEE Transactions on Signal Processing*, vol. 44, no. 6, pp. 1469–1484, June 1996.

[29] P. Stoica and R. L. Moses, *Spectral Analysis of Signals*. Upper Saddle River, NJ: Prentice-Hall, 2005.

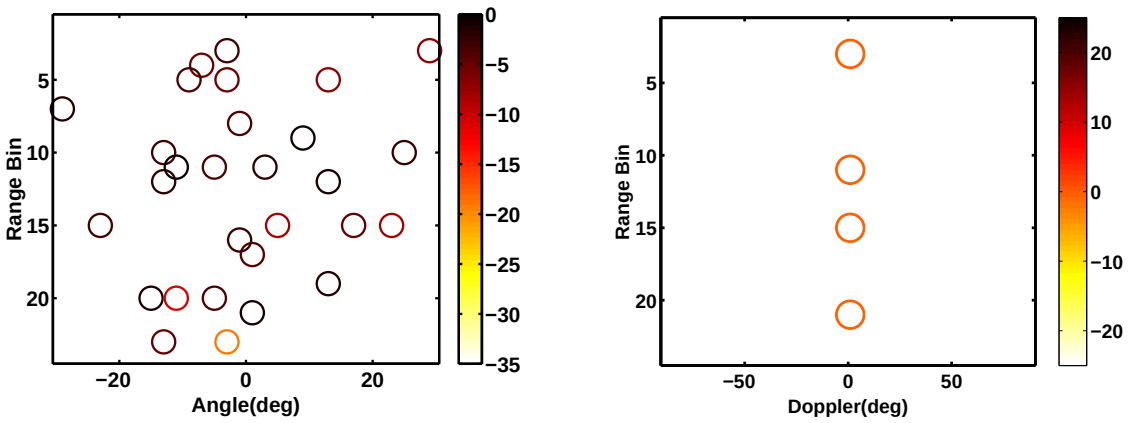

(a) (b)

Fig. 1. True target images for: (a) negligible Doppler examples and (b) non-negligible Doppler examples.

[30] P. Stoica and Y. Selén, "Model-order selection: a review of information criterion rules," *IEEE Signal Processing Magazine*, vol. 21, no. 4, pp. 36–47, July 2004.

[31] C. V. Jakowatz, Jr., D. E. Wahl, P. H. Eichel, D. C. Ghiglia, and P. A. Thompson, *Spotlight-Mode Synthetic Aperture Radar: A Signal Processing Approach*. Norwell, MA: Kluwer Academic Publishers, 1996.

[32] W. G. Carrara, R. S. Goodman, and R. M. Majewski, *Spotlight Synthetic Aperture Radar Signal Processing Algorithms*. Norwood, MA: Artech House Inc., 1995.

[33] J. G. Proakis, *Digital Communications*. McGraw-Hill Inc., third edition, 1995.

[34] J. Li, P. Stoica, and X. Zheng, "Signal synthesis and receiver design for MIMO radar imaging," *IEEE Transactions on Signal Processing*, vol. 56, no. 8, pp. 3959–3968, August 2008.

[35] I. F. Gorodnitsky and B. D. Rao, "Sparse signal reconstruction from limited data using FOCUSS: A re-weighted minimum norm algorithm," *IEEE Transactions on Signal Processing*, vol. 45, no. 3, pp. 600–616, 1997.

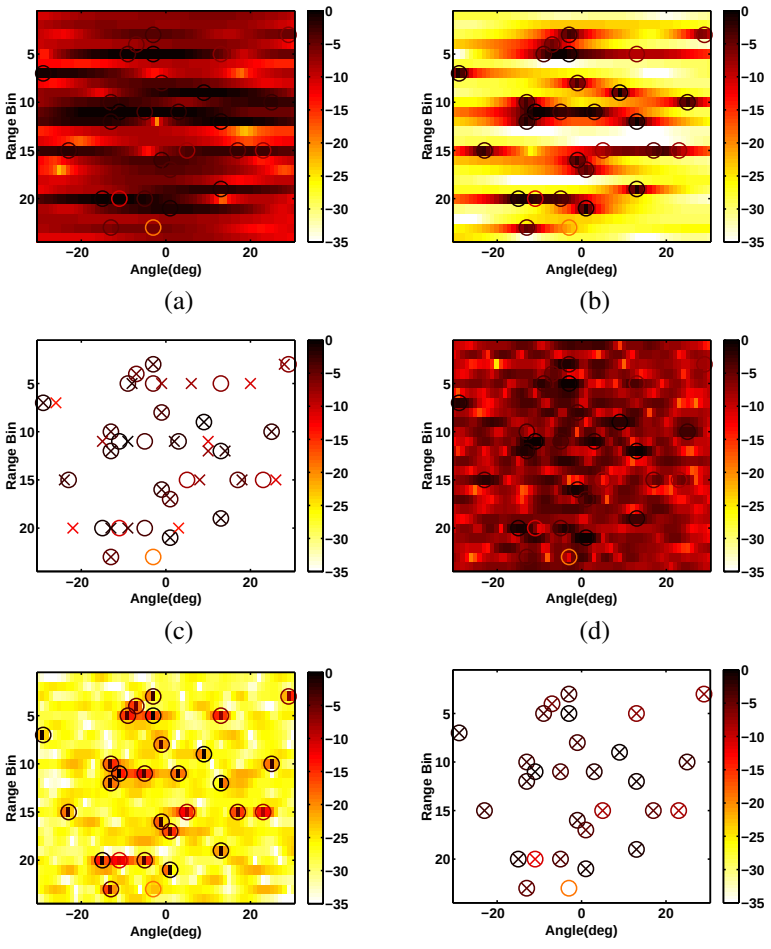

Fig. 2. Spotlight SAR images for $\tilde{N}$=1, $L = 64$ and SNR = 20 dB: (a) DAS with a SIMO array, (b) IAA-R with a SIMO array, (c) IAA-R with a SIMO array and BIC applied, (d) DAS with a MIMO array, (e) IAA-R with a MIMO array and (f) IAA-R with a MIMO array and BIC applied. All levels shown are in dB. 'O' denotes a true target and 'X' represents a target estimate.

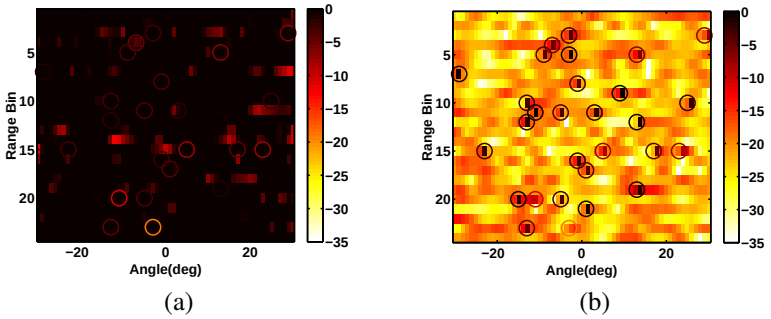

Fig. 3. MIMO SAR images for $\tilde{N}$=1, $L = 64$ and SNR = 20 dB: (a) IAA without regularization and with a scanning grid from -30° to 30° and (b) IAA without regularization and with a scanning grid from -90° to 90°. All levels shown are in dB. 'O' denotes a true target and 'X' represents a target estimate.

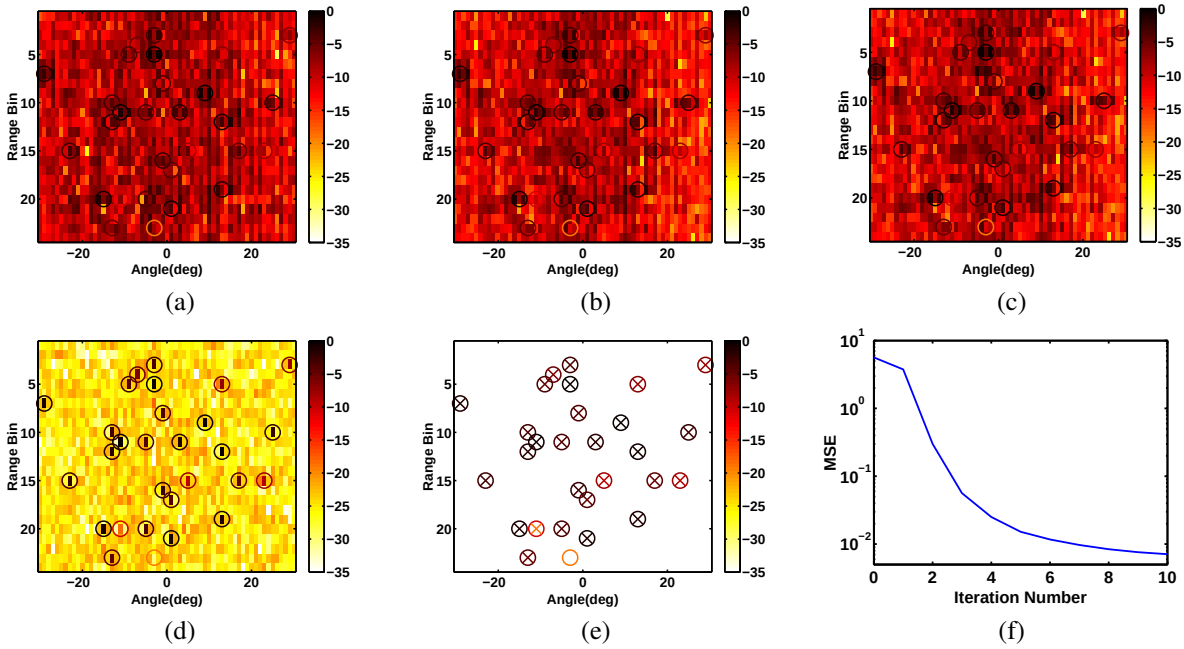

Fig. 4. MIMO SAR images for $\tilde{N}$=3, $L = 32$ and SNR = 15 dB: (a) DAS, (b) Capon, (c) APES, (d) IAA-R and (e) IAA-R with BIC applied. (f) MSE vs. iteration number for IAA-R. The levels shown in (a)-(e) are in dB. 'O' denotes a true target and 'X' represents a target estimate.

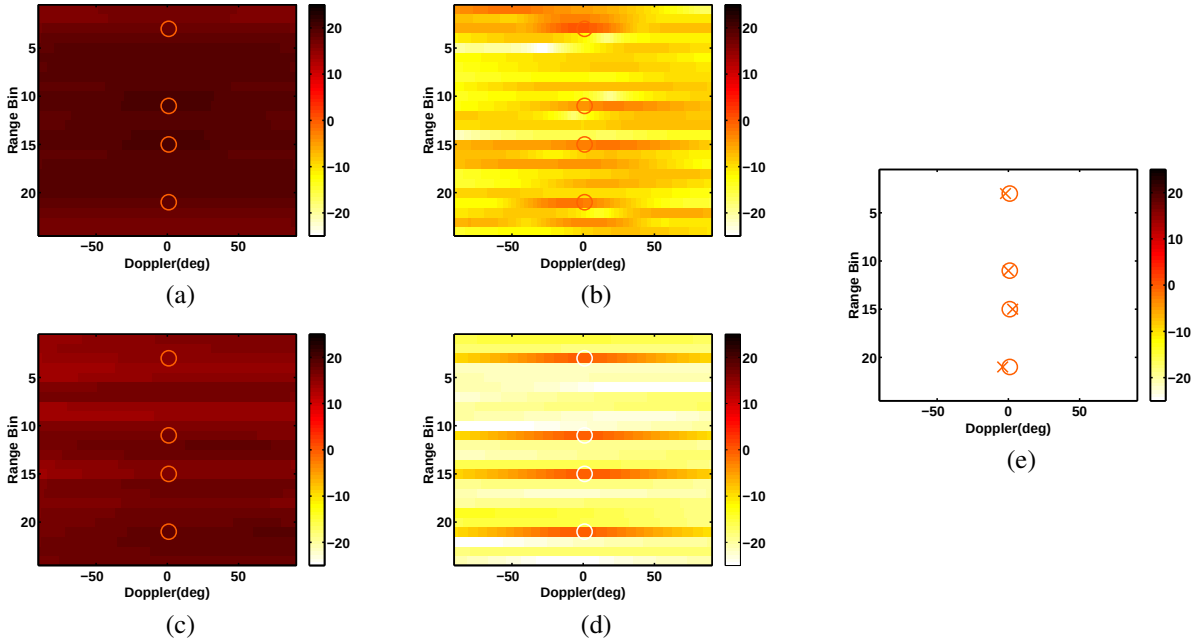

Fig. 5. Range-Doppler images at 1° relative to a broadside scan for $L = 32$ and SNR = 20 dB: (a) DAS with a SIMO array, (b) IAA-R with a SIMO array, (c) DAS with a MIMO array, (d) IAA-R with a MIMO array and (e) IAA-R with a MIMO array and BIC applied. All levels shown are in dB. 'O' denotes a true target and 'X' represents a target estimate.

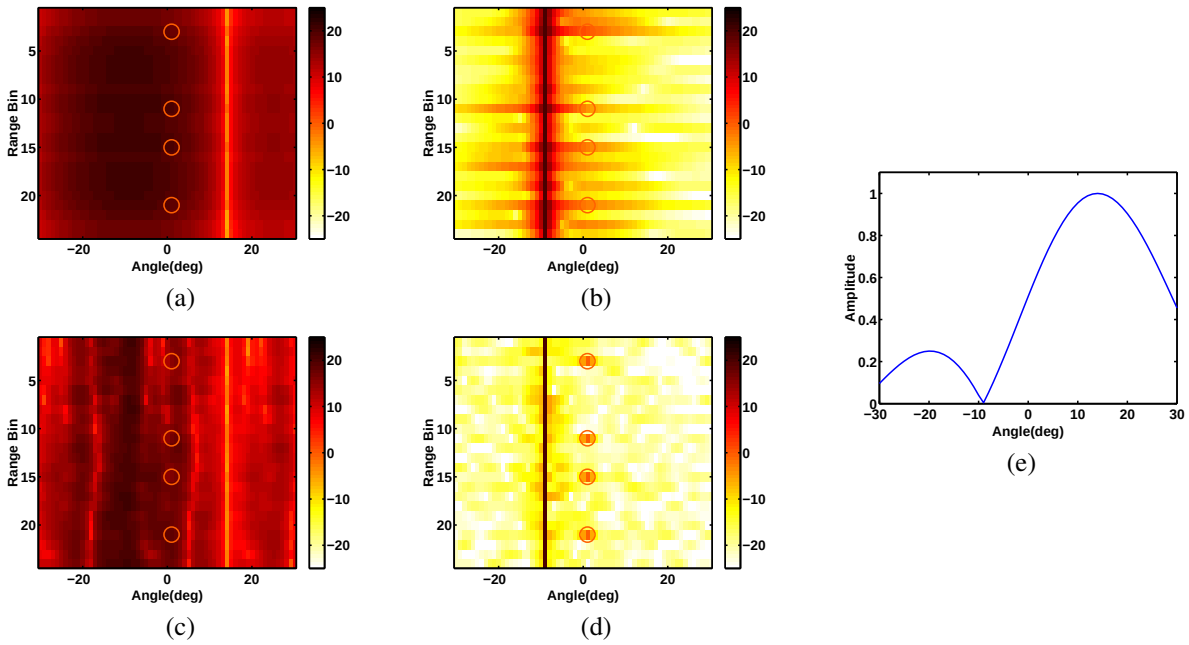

Fig. 6. Angle-range images at 1° Doppler for $L = 32$ and SNR = 20 dB: (a) DAS with a SIMO array, (b) IAA-R with a SIMO array, (c) DAS with a MIMO array and (d) IAA-R with a MIMO array. (e) Receive filter response for images (a) and (c). Levels shown for (a)-(e) are in dB and for (f) in amplitude. 'O' denotes a true target.

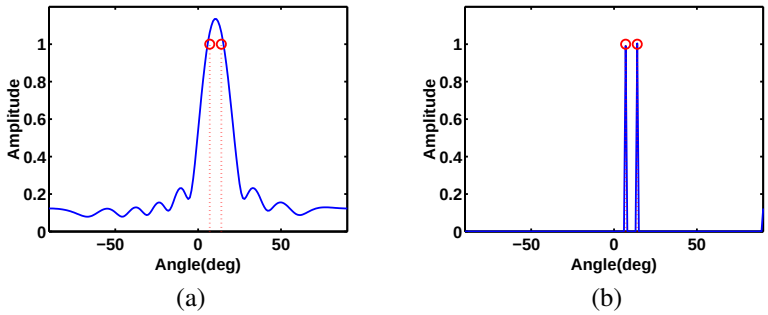

Fig. 7. Passive array target estimates for $N = 10$ using: (a) DAS and (b) IAA. 'O' denotes a true target location.

Jian Li (S'87-M'91-SM'97-F'05) received the M.Sc. and Ph.D. degrees in electrical engineering from The Ohio State University, Columbus, in 1987 and 1991, respectively.

From April 1991 to June 1991, she was an Adjunct Assistant Professor with the Department of Electrical Engineering, The Ohio State University, Columbus. From July 1991 to June 1993, she was an Assistant Professor with the Department of Electrical Engineering, University of Kentucky, Lexington. Since August 1993, she has been with the Department of Electrical and Computer Engineering, University of Florida, Gainesville, where she is currently a Professor. In Fall 2007, she was on sabbatical leave at MIT, Cambridge, Massachusetts. Her current research interests include spectral estimation, statistical and array signal processing, and their applications.

Dr. Li is a Fellow of IEEE and a Fellow of IET. She is a member of Sigma Xi and Phi Kappa Phi. She received the 1994 National Science Foundation Young Investigator Award and the 1996 Office of Naval Research Young Investigator Award. She was an Executive Committee Member of the 2002 International Conference on Acoustics, Speech, and Signal Processing, Orlando, Florida, May 2002. She was an Associate Editor of the IEEE Transactions on Signal Processing from 1999 to 2005, an Associate Editor of the IEEE Signal Processing Magazine from 2003 to 2005, and a member of the Editorial Board of Signal Processing, a publication of the European Association for Signal Processing (EURASIP), from 2005 to 2007. She has been a member of the Editorial Board of Digital Signal Processing – A Review Journal, a publication of Elsevier, since 2006. She is presently a member of the Sensor Array and Multichannel (SAM) Technical Committee of IEEE Signal Processing Society. She is a co-author of the papers that have received the First and Second Place Best Student Paper Awards, respectively, at the 2005 and 2007 Annual Asilomar Conferences on Signals, Systems, and Computers in Pacific Grove, California. She is a co-author of the paper that has received the M. Barry Carlton Award for the best paper published in IEEE Transactions on Aerospace and Electronic Systems in 2005. She is also a co-author of the paper that has received the Best Student Paper Award at the 2009 SPIE Defense, Security, and Sensing Conference in Orlando, Florida.

William Roberts (S'09) received the B.S. and M.Sc. degrees in electrical engineering from the University of Florida in 2006 and 2007, respectively. He is working towards the Ph.D. degree in the Department of Electrical and Computer Engineering, University of Florida, Gainesville. His research interests include statistical signal processing and radar signal processing. He is a Student Member of the IEEE.

Tarik Yardibi (S'08) received the B.S. degree from Hacettepe University, Ankara, Turkey in 2004 and the M.S. degree from Bilkent University, Ankara, Turkey in 2006, both in electrical engineering. He is currently pursuing the Ph.D. degree at the Spectral Analysis Laboratory at University of Florida, Gainesville. His research interests include statistical signal processing, sensor array processing, aeroacoustic measurements and sparse signal representations.

Petre Stoica (F'94) received the D.Sc. degree in automatic control from Polytechnic Institute of Bucharest (BPI), Bucharest, Romania, in 1979 and an honorary doctorate degree in science from Uppsala University (UU), Uppsala, Sweden, in 1993.

He is a professor of systems modeling with the Division of Systems and Control, the Department of Information Technology at UU. Previously, he was a professor of system identification and signal processing with the Faculty of Automatic Control and Computers at BPI. He held longer visiting positions with Eindhoven University of Technology, Eindhoven, The Netherlands; Chalmers University of Technology, Gothenburg, Sweden (where he held a Jubilee Visiting Professorship); UU; the University of Florida, Gainesville, FL; and Stanford University, Stanford, CA. His main scientific interests are in the areas of system identification, time series analysis and prediction, statistical signal and array processing, spectral analysis, wireless communications, and radar signal processing.

Dr. Stoica has published nine books, ten book chapters, and some 500 papers in archival journals and conference records. The most recent book he coauthored, with R. Moses, is Spectral Analysis of Signals (Prentice-Hall, 2005). He is on the editorial boards of six journals: the Journal of Forecasting; Signal Processing; Circuits, Signals, and Signal Processing; Digital Signal Processing: A Review Journal; Signal Processing Magazine; and Multidimensional Systems and Signal Processing. He was a co-guest editor for several special issues on system identification, signal processing, spectral analysis, and radar for some of the aforementioned journals, as well as for IEE Proceedings. He was corecipient of the IEEE ASSP Senior Award for a paper on statistical aspects of array signal processing. He was also recipient of the Technical Achievement Award of the IEEE Signal Processing Society. In 1998, he was the recipient of a Senior Individual Grant Award of the Swedish Foundation for Strategic Research. He was also co-recipient of the 1998 EURASIP Best Paper Award for Signal Processing for a work on parameter estimation of exponential signals with time-varying amplitude, a 1999 IEEE Signal Processing Society Best Paper Award for a paper on parameter and rank estimation of reduced-rank regression, a 2000 IEEE Third Millennium Medal, and the 2000 W. R. G. Baker Prize Paper Award for a paper on maximum likelihood methods for radar. He was a member of the international program committees of many topical conferences. From 1981 to 1986, he was a Director of the International Time-Series Analysis and Forecasting Society, and he was also a member of the IFAC Technical Committee on Modeling, Identification, and Signal Processing. He is also a member of the Royal Swedish Academy of Engineering Sciences, an honorary member of the Romanian Academy, and a fellow of the Royal Statistical Society.

Firooz A. Sadjadi received the BSEE from Purdue University in 1972, MSEE in 1974, and the DEE in 1976 from the University of Southern California (USC). He worked at the USC Image Processing Institute and the Image and Pattern Analysis Laboratory of the University of Tennessee, and was a consultant to the Oak Ridge National Laboratory. During 1983-1993, he was with the Honeywell systems and Research Center as a principal research scientist. In 1993 he joined the Lockheed Martin Corporation where he is a senior research staff scientist. His interests are in theoretical and experimental research related to signal and image processing, pattern recognition, target tracking and information fusion.

He was the Guest Editor for the Optical Engineering Journal Special Issues on Performance Evaluations of Signal and Image Processing Systems, February 1991, Automatic Target Recognition, December 1992, and for the IEEE Computer Special Section on Applications of Computer Vision, July 1997. He currently serves on the Editorial Board of the Information Fusion Journal. He is the author of more than 150 journal and conference publications, is an author of 7 book chapters, and holds 10 US and International Patents. He is the editor of several books, Automatic Target Recognition Systems (2000), Sensor and Data Fusion (1996), Performance Evaluations of Signal and Image Processing Systems (1993), and The Physics of Automatic Target Recognition published by Springer in 2007. He has served on a number of governmental and academic research panels and currently serves as the Twin Cities Chapter of the IEEE Aerospace and Electronic Systems Society. He has received a number of technical awards including the Honeywell Technical Achievement Award, and the Lockheed Martin Evening of the Stars Award. He is a Fellow of the International Society for Optical Engineering (SPIE), is a Senior Member of the IEEE, and is a member of Sigma Xi, Optical Society of America and Mathematical Association of America.